NCAR/TN-147+STR
NCAR TECHNICAL NOTE

November 1979

Case Studies on Convective Storms
Case Study 4

27 July 1976: First Echo Case

Daniel W. Breed

CONVECTIVE STORMS DIVISION

NATIONAL CENTER FOR ATMOSPHERIC RESEARCH
BOULDER, COLORADO

FOREWORD

This is one of a series of Technical Notes reporting data on aircraft penetrations in convective clouds, ranging from cumulus congestus to thunderstorms, in northeastern Colorado and adjacent portions of Wyoming and Nebraska. The June and July 1976 field season of the National Hail Research Experiment is the setting of the first six to ten of these Notes. The series may be extended later to the 1974, 1975 and 1978 seasons. All of the cases involve aircraft data, including vertical velocity, state parameters and cloud physical data, obtained in coordination with detailed S-band radar scans, normally taken with about two minute time resolution.

Some of these cases will be the subject matter of formal publications, in which case the Tech Note will supplement the publication by providing a more extensive presentation of data. Other cases will be presented as complete sets of data only in the Tech Notes, but usually some portions of the data will be included in publications on general properties of convective clouds over the high plains.

These Tech Notes will always have the following components: a brief synoptic setting, a representative sounding, a brief, general radar reflectivity history, a more detailed radar history of the cloud or storm investigated with the aircraft tracks superimposed, a presentation of the aircraft data, and a discussion. The presentation will not be truly complete either as regards radar data or cloud droplet or precipitation particle size spectra, because these data are too voluminous. However, the general data, such as particle concentrations and

liquid water content, will be presented along with some examples of the more complete data and remarks on typical aspects.

The data quality is in some cases difficult to assess. There is no absolute standard for many in-cloud measurements, even of temperature. Trust in the listed values for liquid water content and droplet sizes and concentrations must always be qualified to some degree. These Technical Notes will include remarks on data quality that record the opinions of those closest to taking the data, and the reasons for the opinions. Work on the data reliability will be continuing, however, and because of this, some of these opinions may change. Any such changes will be recorded in the Tech Note series, along with reference to previous notes in which changes should be made.

The penetrating aircraft for the 1976 season were the NCAR/NOAA sailplane, the University of Wyoming Queen Air, and the South Dakota School of Mines and Technology armored T-28.

This series of Tech Notes is intended to provide a lasting record of cloud data in the high plains area that may be of use in unforeseeable ways in future atmospheric studies. The data were gathered as part of the National Hail Research Experiment, managed by the National Center for Atmospheric Research and sponsored by the Weather Modification Program, Research Applications Directorate, National Science Foundation.

Charles A. Knight
June 1978

ACKNOWLEDGMENTS

I would like to thank Charlie Knight for his helpful comments on the manuscript. The Research Aviation Facility of NCAR provided the Queen Air 306D data.

CONTENTS

LIST OF FIGURES

ABSTRACT

On 27 July 1976, a relatively small, weak storm was investigated by the NCAR/NOAA instrumented sailplane in coordination with NCAR Queen Air 306D. The potential instability was weak on this day, and the investigated storm probably was initiated from the observed surface convergence which resulted from outflow of an older storm to the northwest and/or surface topography. The sailplane made an extended penetration from 1635 to 1715 covering ∿3400 m in altitude with weak updrafts initially, growing to moderately strong updrafts and then finally weak downdrafts. Ice particle concentration and size both increased throughout the penetration to about 100 ℓ^{-1} and 2-4 mm graupel. The Queen Air measured fairly weak updrafts at cloud base and mixed thermodynamic conditions. Later subcloud passes (∿1700) revealed decaying conditions, weak downdrafts and lower θ_e values. The storm had the characteristic life cycle of a simple rainshower.

I. METEOROLOGICAL SYNOPSIS

The low-level synoptic conditions at 1500 MDT shown in Fig. 1 were dominated by a rapidly developing low pressure center in southwestern South Dakota and its associated trough and frontal surface through western Nebraska. These features caused an accentuated northwesterly flow across the NHRE area (shaded area in Fig. 1) and relatively dry conditions (mixing ratios of 6-7 g kg^{-1}), although there was an increase in moisture through the eastern half of the NHRE area. The moist southerlies across Kansas were not pronounced on this day, and did not extend into northeastern Colorado to affect the research area.

The 500 mb NMC analysis at 1800 MDT of the 27th (Fig. 2) shows weak mid-level winds across the NHRE area, and a strong short-wave through the Dakotas and across the High Plains. This is associated with the development of the surface low in South Dakota. The influence of the low pressure center in Canada is reflected at the surface in the trailing cold front across northern Wyoming, shown in Fig. 1.

The closest sounding to the first echo investigation, spatially and temporally, is the 1553 MDT Grover release, shown in Fig. 3. The 7 g kg^{-1} mixing ratio line, the 317 K potential temperature (θ) line, and the 337 K equivalent potential temperature (θ_e) line are plotted for reference and the θ_e trace for the entire sounding is inserted in the upper left corner of Fig. 3. Wind speed and direction are plotted along the right side at 1 km intervals,[1] and show light winds with very

[1] All heights are referenced to mean sea level and times are referenced to Mountain Daylight Time (MDT).

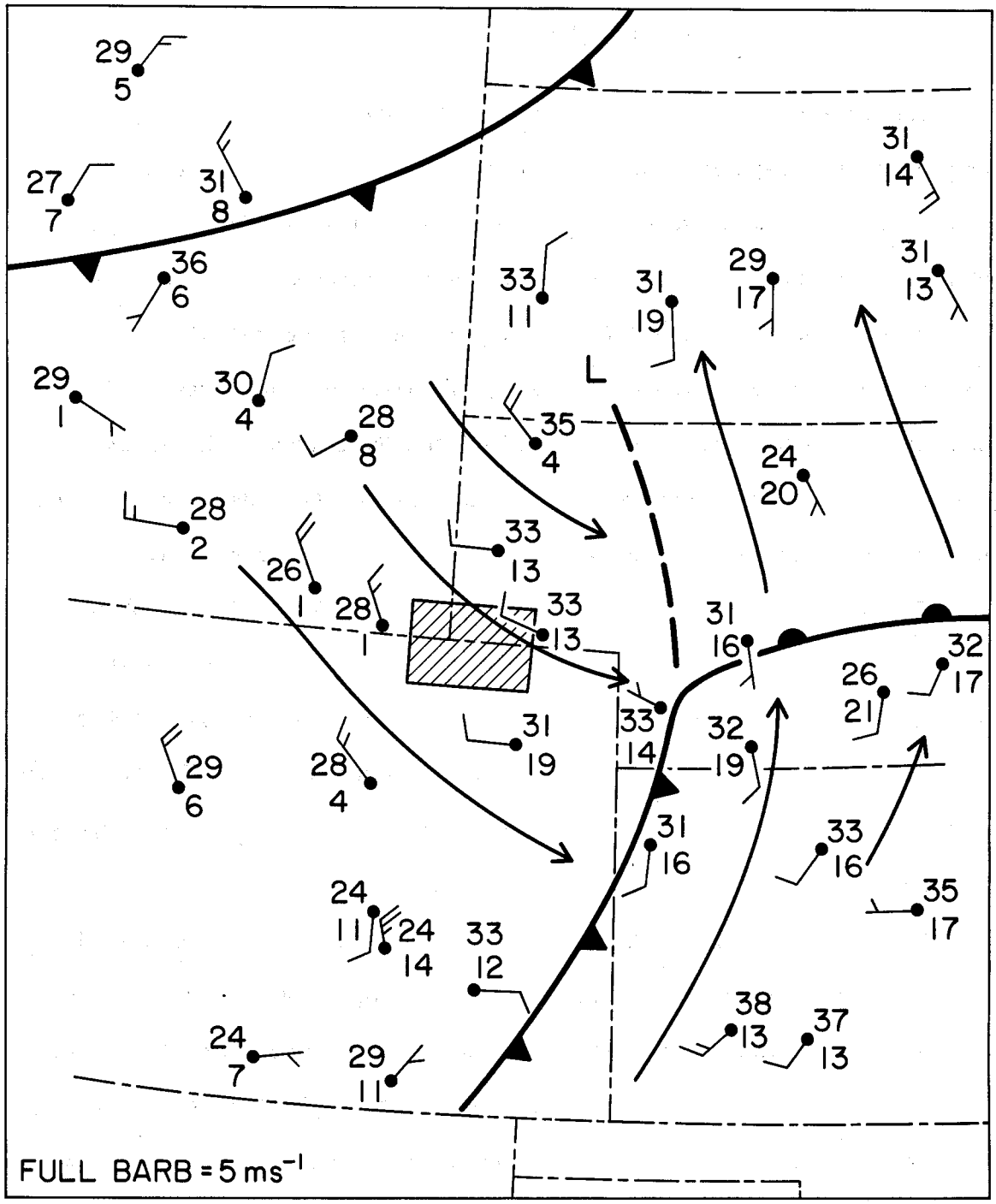

SURFACE ANALYSIS 27 JULY 1976 1500 MDT

Fig. 1. Regional surface map for 1500 MDT on 27 July 1976 showing the synoptic scale conditions shortly before the first echo investigation. The NHRE research area is shaded. Temperature (°C), dew point (°C), wind speed and direction are plotted at each station.

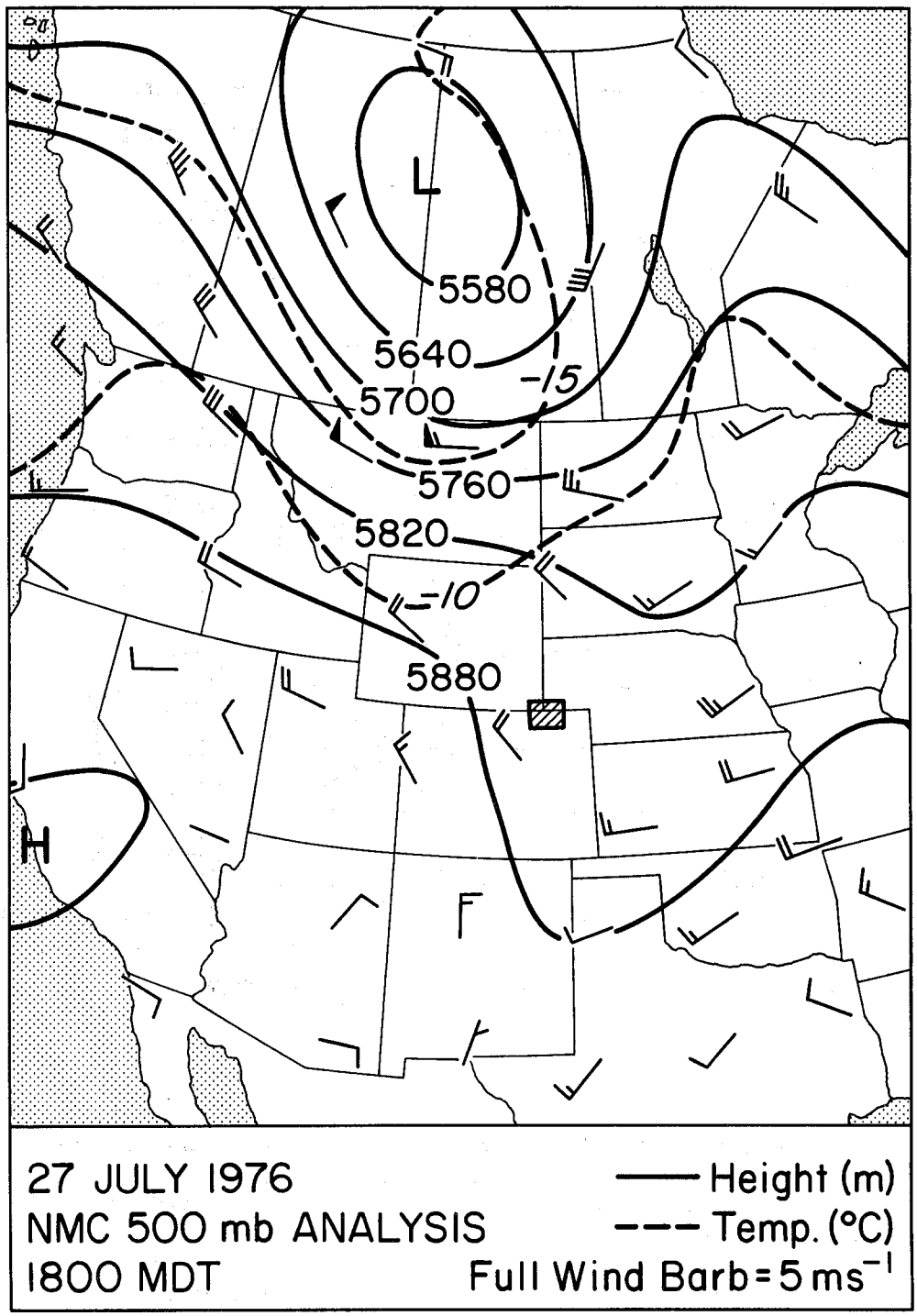

Fig. 2. 500 mb map of the western U.S. showing the 1800 MDT NMC analysis of the mid-level synoptic conditions on 27 July 1976. Solid lines are geopotential height contours (m) every 60 m; dashed lines are isotherms (°C) every 5°C; and wind vectors are plotted at each of the upper air stations. The NHRE research area is shaded.

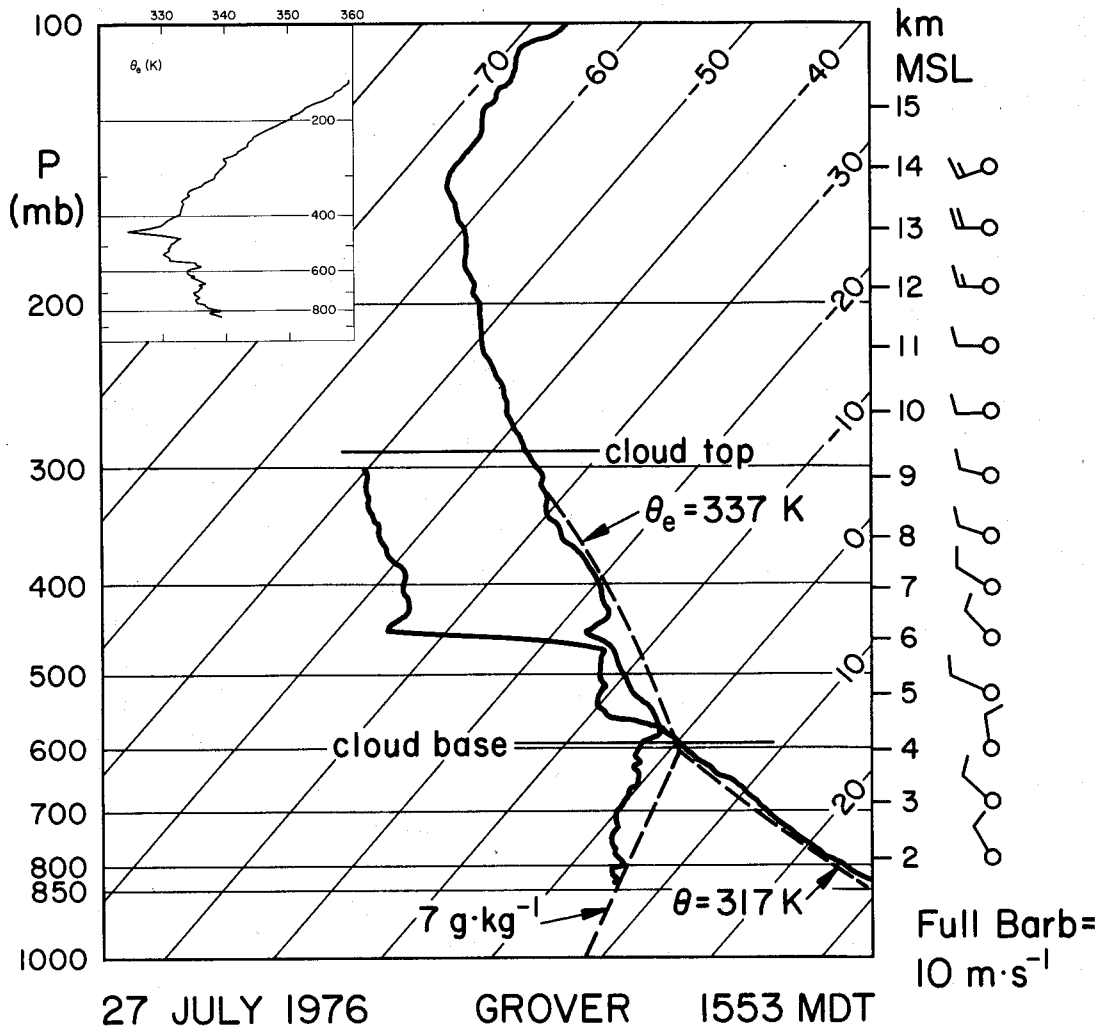

Fig. 3. Thermodynamic diagram showing the vertical distribution of temperature and dew point from the Grover 1553 sounding. Selected dry and moist adiabats and mixing ratio have been plotted as dashed lines and labeled. Winds are plotted every kilometer; full barb is 10 m s^{-1}. Insert in the upper left shows θ_e vs. pressure for this sounding. Queen Air-measured cloud base and radar-measured cloud top are also indicated.

little shear through the troposphere. This sounding shows slightly cooler and drier conditions in the lower levels than those detected by cloud base aircraft which reported cloud base at 595 mb (4.4 km) with θ values of 316-317 K, θ_e values of ~337 K, and mixing ratio values of 6.5-7 g kg^{-1}. The upper levels of the sounding show fairly stable conditions with a lifted index at 500 mb of only 1-1.5°C. The first echo storm environment was probably less stable than shown in the sounding, however, since the radar top of the sailplane-penetrated cloud reached 9.7 km during the investigation and tops of cells north of the investigated region reached 11-11.5 km. A parcel lifted moist adiabatically at θ_e = 337 K only predicts a top of slightly less than 9 km. The inversion at 450 mb was a persistent feature in all the soundings, including those at the Potter and Sterling sites, up to the time of this sounding after which it was no longer a distinctive feature. Surface observations and photographs earlier in the day indicate that the many cumulus humilis that formed were suppressed, presumably due to this stable layer.

An example of some of the data available from the Portable Automated Mesonet (PAM) stations is shown in Fig. 4, including wind vectors, θ, θ_e, and mixing ratio (M.R.) for each station. The mesoscale network also included 31 conventional mesoscale stations, and those data are available on strip charts but have not been reduced or calibrated. A PPI map at 5.8° elevation angle is included in Fig. 4 with the first echo area marked by an X. A cursory analysis of the mesonet data shows a well-defined convergence line (marked by a dashed line in Fig. 4) between the northerly to northwesterly flow across the northern half

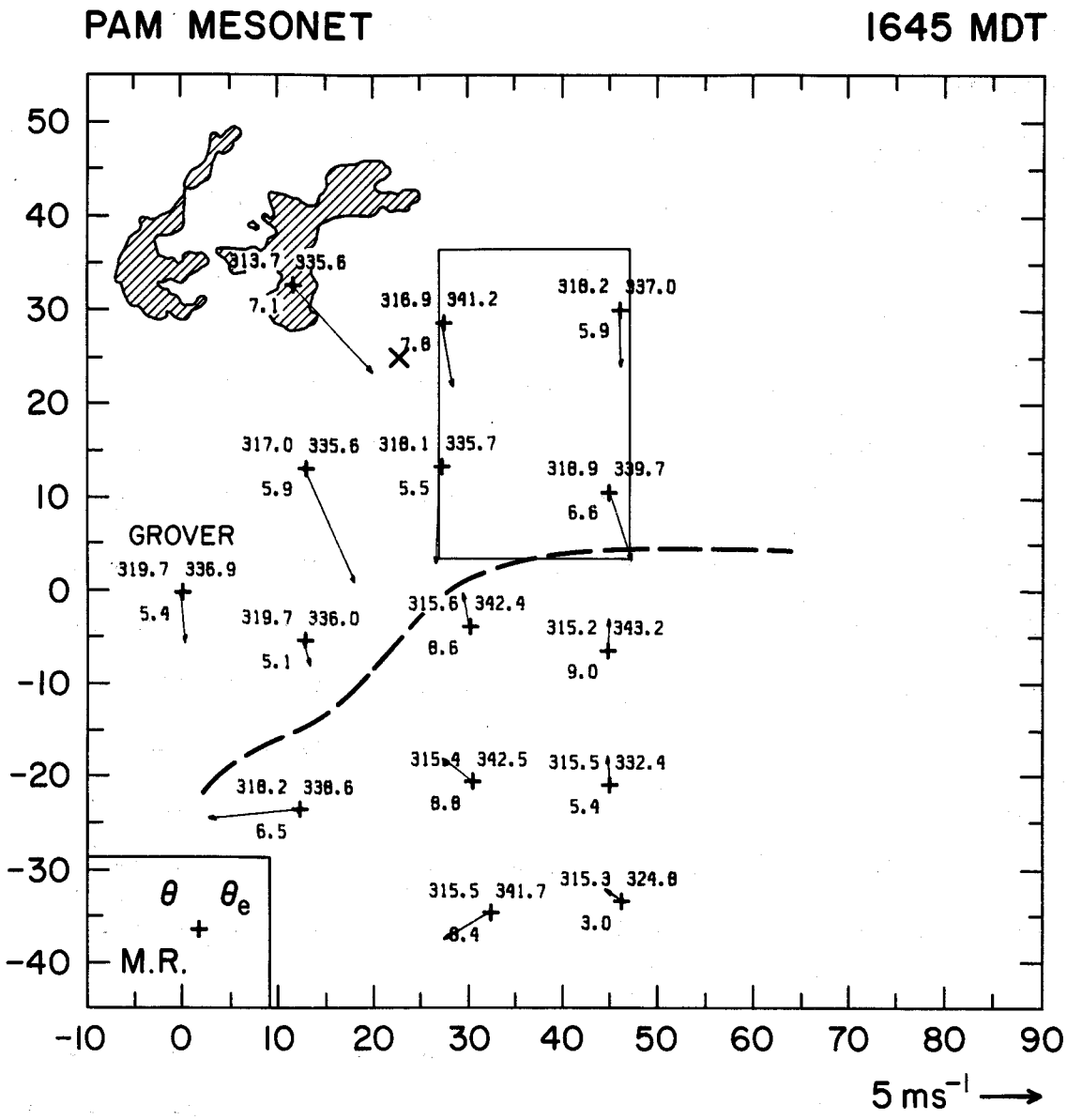

Fig. 4. Map of the NHRE research area showing the 1645 data from the PAM mesonet stations. θ, θ_e, mixing ratio and wind vectors are plotted at each station. Solid box in middle of area marks the boundary of the dense precipitation network. Shaded area is radar echo >15 dBZ from Grover radar PPI at 5.8° elevation angle. First echo investigation area is marked with an X. Dashed line marks convergence of northerly and southerly wind regimes.

of the network and the southerly to southeasterly flow in the southern half. The northwesterly flow of the synoptic conditions is accentuated by outflow from the northwestern storm across the network while the southerly flow is probably enhanced by an upslope circulation of the elevated plateau east of Grover. No significant convection was associated with this convergence line however. The winds appear to be convergent in the first echo area at 1645, although by 1700 outflow from the first echo storm and the older northwestern storm is reflected at the surface and shows divergence in this area. The strong surface winds associated with the outflow can be followed as they propagate across the network. The reduced and calibrated PAM data are available on microfilm for the time period 1400-2000, and with the conventional mesonet data can detail the surface mesoscale conditions in which the first echo storm formed and propagated.

Weak synoptic conditions existed on this day with moderate mixing ratios, fairly stable thermodynamic conditions, and weak westerlies. The first echo storm was probably initiated in response to the mesoscale influences of nearby storms and/or elevated terrain. Although the day did not produce very intense convection, there was small hail recorded at a number of stations in the precipitation network. The storm studied in this report produced only a trace amount of precipitation at one station.

II. RADAR SUMMARY

The storm of interest in this study developed about 30 km northeast of Grover and intensified rather quickly, then dissipated slowly as it propagated southeastward across the southern half of the dense precipitation network. Its initial formation took place within 10 km to the southeast of an older storm mass. Figure 5a[2] is a radar PPI of the older storm about 5 min prior to the first echo of the cells associated with the investigated storm. The eastern-southeastern area of the echo mass was still active, and it was downwind of this area that a group of new cells formed into a separate system. NCAR Queen Air 306D began its investigation at about this time (1630). At 1645, the northeastern-most cell in the group can be seen, as marked with an arrow in Fig. 5b, while cells to the southwest were in the first echo stage, detectable at a higher elevation angle than this PPI. The sailplane was spiralling in a consistent, moderately strong updraft immediately southwest of the cell shown at this time. Figure 5c shows the development that had taken place in the group of cells investigated by the aircraft by 1700. The sailplane was at the top of its climb in an updraft near the cell marked with an arrow. The cells of this storm maintained their discreteness at the higher altitudes while the radar echo at the lower altitudes had merged. The storm maintained its identity past 1730 at which time the radar operations were shifted to concentrate on another storm. Although this storm reached 50 dBZ for a short time

[2] All radar plots have the Grover radar at the origin of the coordinate system. For specifications of the Grover radar, see Appendix A.

near cloud base, no precipitation was recorded at any of the stations under its path as it propagated southeastward across the dense precipitation network. A trace amount of precipitation was recorded between 1645 and 1700 under the northeastern cell while it was still developing. Remnants of the investigated storm can be seen at the southern end of the dense precipitation network at 1730 in Fig. 5d. The earlier storm initially northwest of the investigated group of cells dissipated as it moved southeastward, and only a small area of weak reflectivity is detectable in Fig. 5d near the middle of the western boundary of the dense precipitation network.

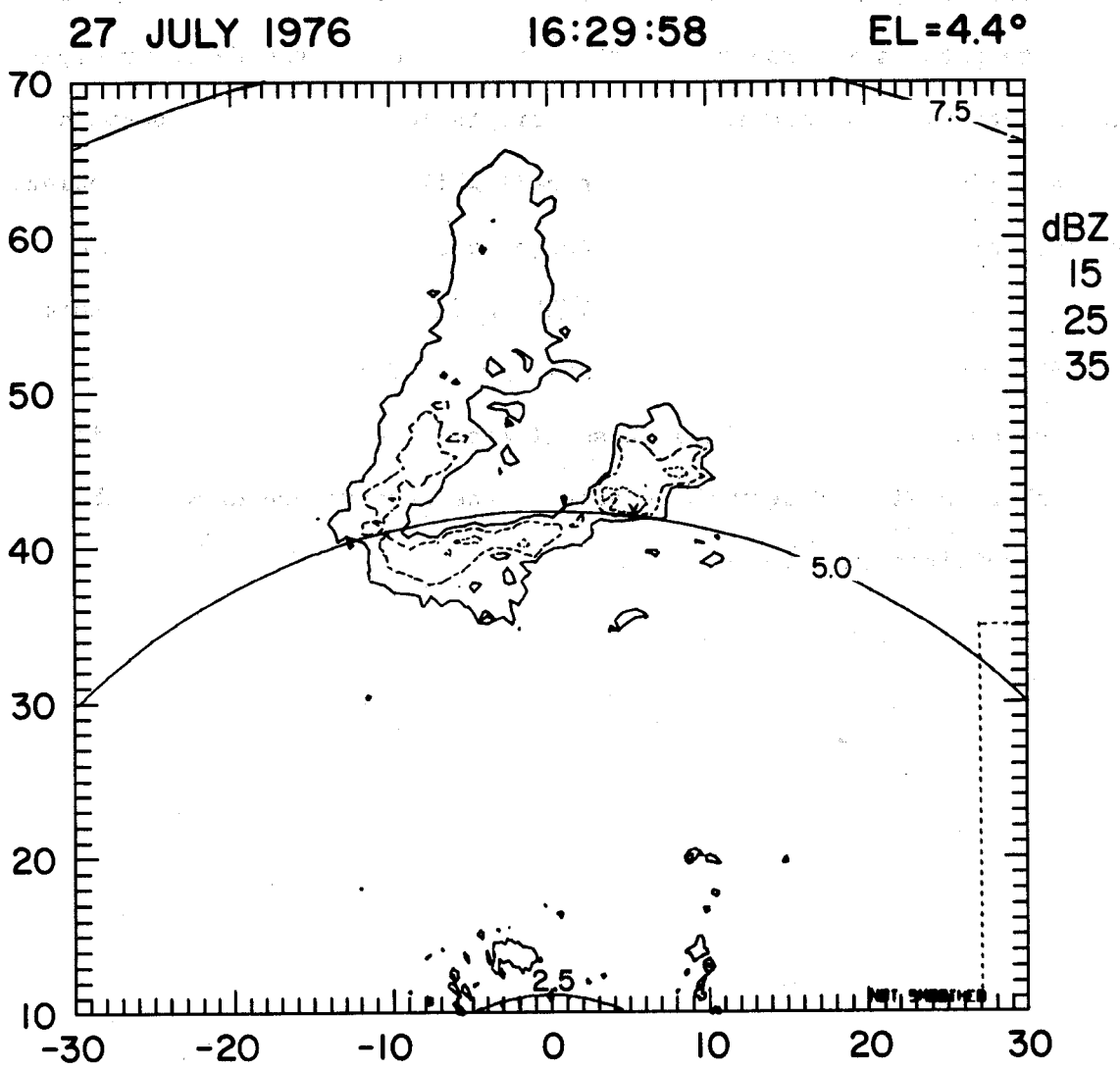

Fig. 5a. The 1629:58 PPI radar scan on 60 km x 60 km map showing reflectivity contours at 4.4° elevation angle on 27 July 1976. Contours are at 10 dBZ intervals from 15 dBZ, and constant altitude arcs are plotted at 2.5, 5.0 and 7.5 km. Dashed lines in lower right corner mark the northern and western boundaries of the dense precipitation network. Note that ground clutter has not been removed from these PPI plots.

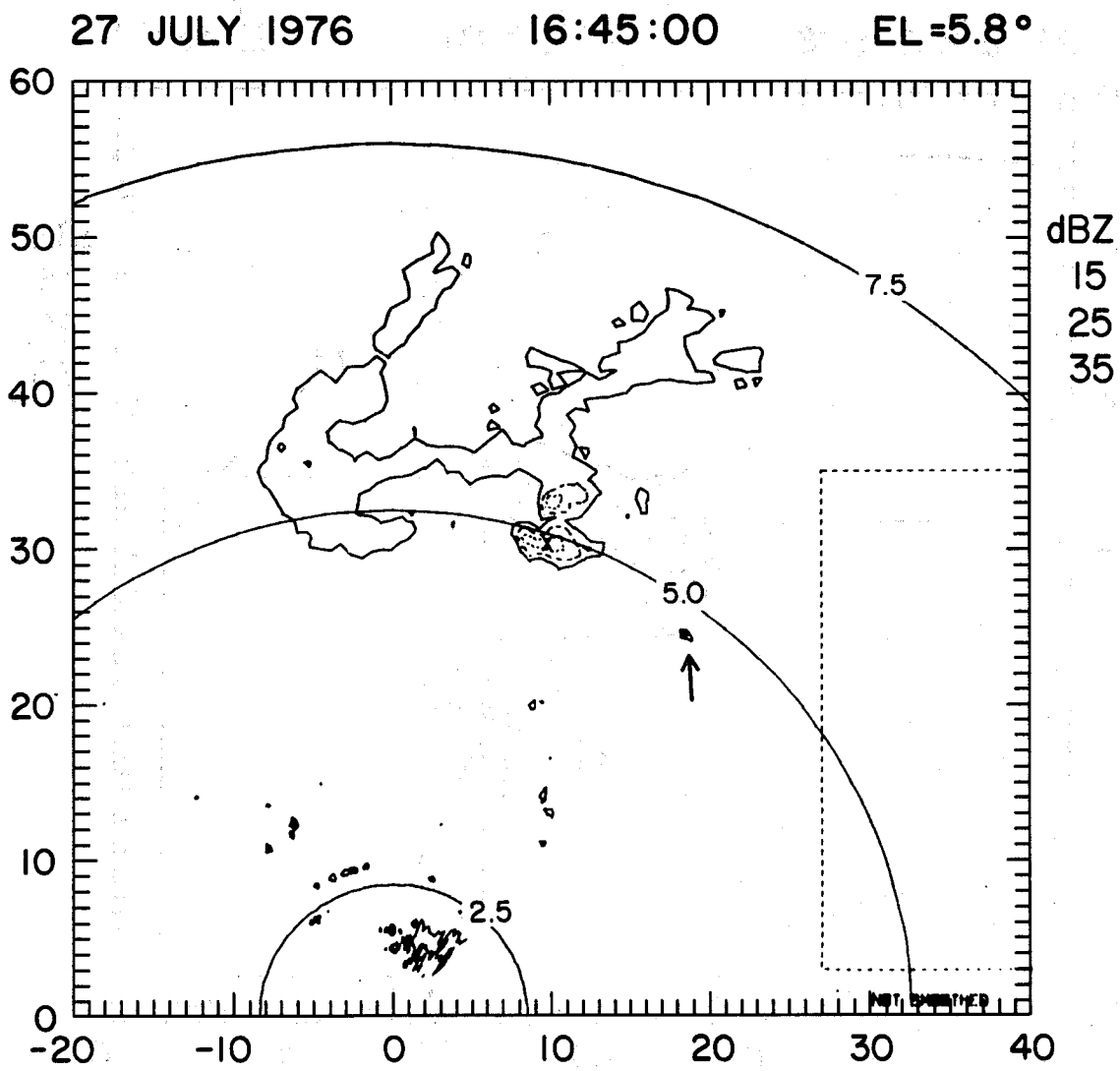

Fig. 5b. Same as 5a except for 1645:00 and 5.8° elevation angle. Area is shifted 10 km south and 10 km east from Fig. 5a, and more of the dense precipitation network is shown. Sailplane investigation (skin-paint) is marked with an arrow.

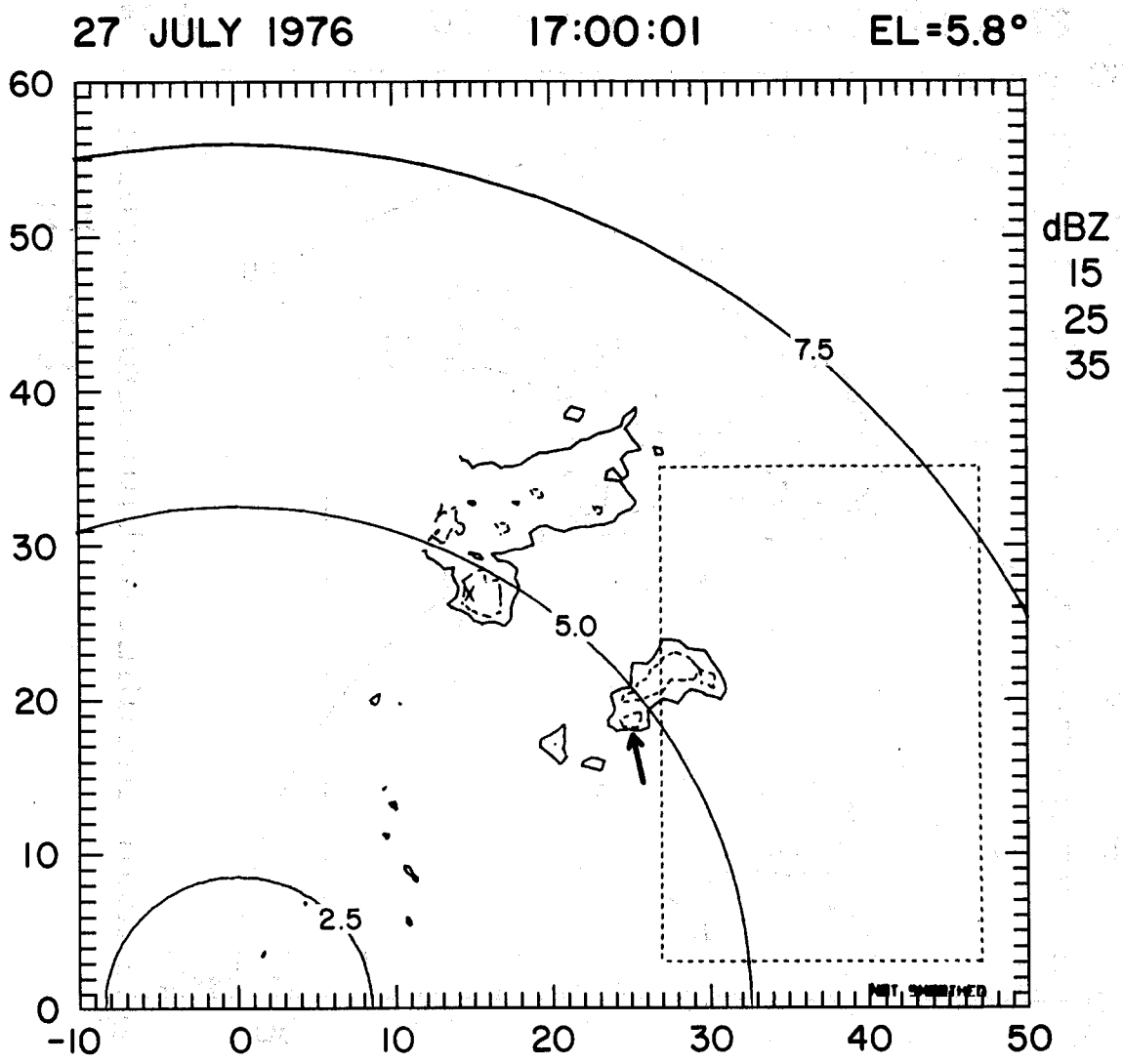

Fig. 5c. Same as 5b except for 1700:01. Area is shifted 10 km east from Fig. 5b, and radar scan limits cut off data from the western side of the older northwestern storm. Arrow marks the cell closest to the sailplane penetration.

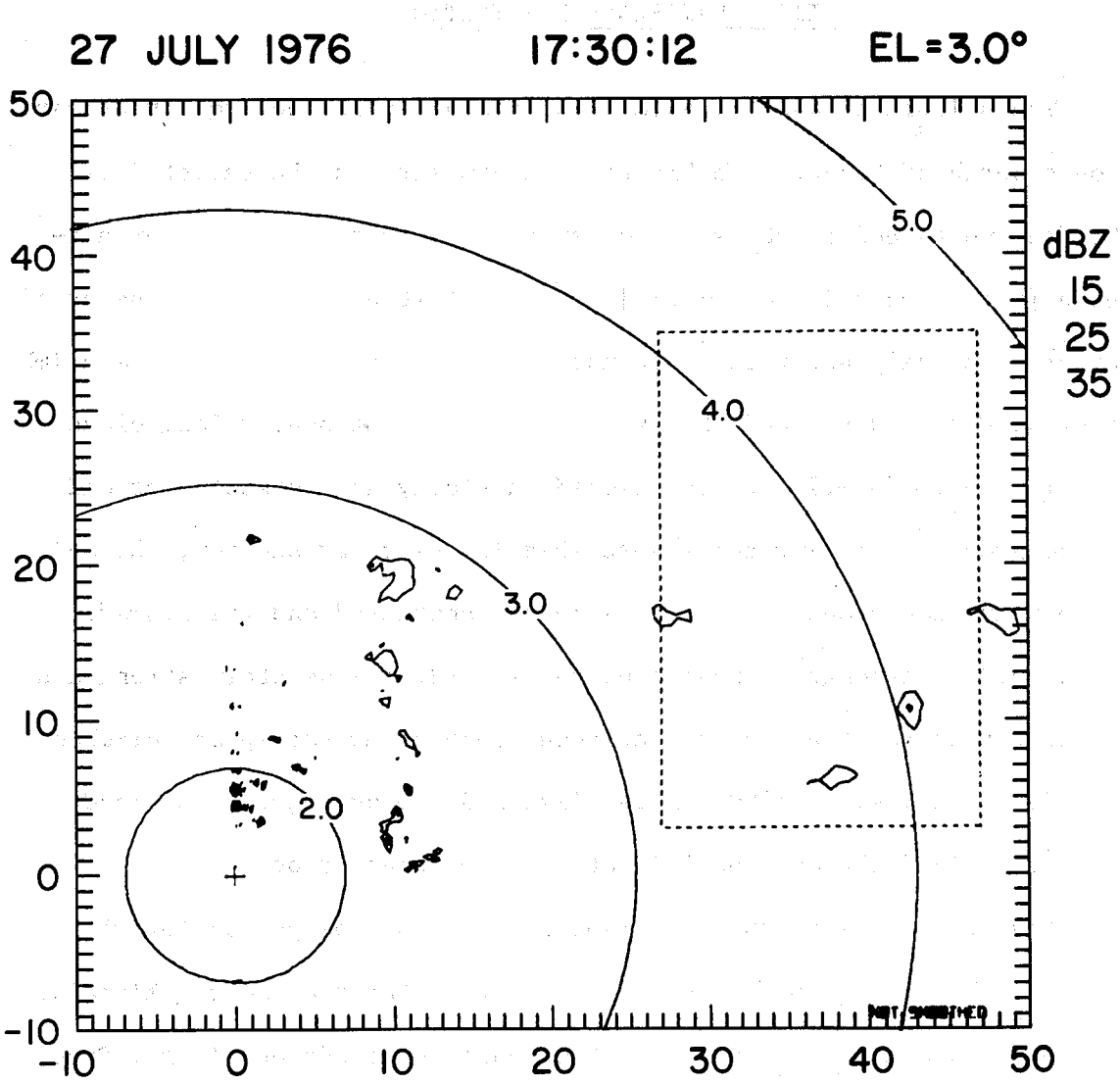

Fig. 5d. Same as 5b except for 1730:12 and 3.0° elevation angle. Area is shifted 10 km south from Fig. 5c, and constant altitude arcs are at 2.0, 3.0, 4.0 and 5.0 km.

III. SAILPLANE PENETRATION

The sailplane, 29J, released from tow at about 1605 to investigate clouds north of Grover. Unable to maintain lift in the selected clouds, 29J flew north and northeast in order to be closer to the Butler airstrip [Grover coordinates (2,21)]. At about 1630 and 7 km northeast of Butler, the sailplane found weak updrafts capable of supporting a climb to cloud base and started what was to be an exceptionally long cloud penetration (∿1635-1715). Positioned initially at the southwest end of the group of growing cells described in the radar section, the sailplane found the cloud conditions somewhat scattered and the updraft diminished in strength. Moving northeastward, a moderately strong and consistent updraft was located at about 1645 and the sailplane climbed from 3.4 to 8.1 km by 1700. This climb and the subsequent in-cloud descent yielded the most useful data of the penetration.

Figures 6a-f show the sailplane's track for the period 1643-1715. These tracks have been shifted 1 km west to match the radar "skinpaint" of the sailplane, which was evident on numerous occasions (e.g., Figs. 6a, b, and c). A variable cell motion (8-10 m s^{-1} to the southeast) has also been included in the track correction, and the resulting track should be within several hundred meters of true position. The radar reflectivity structure from figure to figure is somewhat discontinuous because of the rapid growth and spread of the echo and the variable elevation angles of the PPI's, selected to represent the sailplane altitude as well as possible. However, the general features of the radar echo that occurred at the time and altitude of the different tracks are fairly represented.

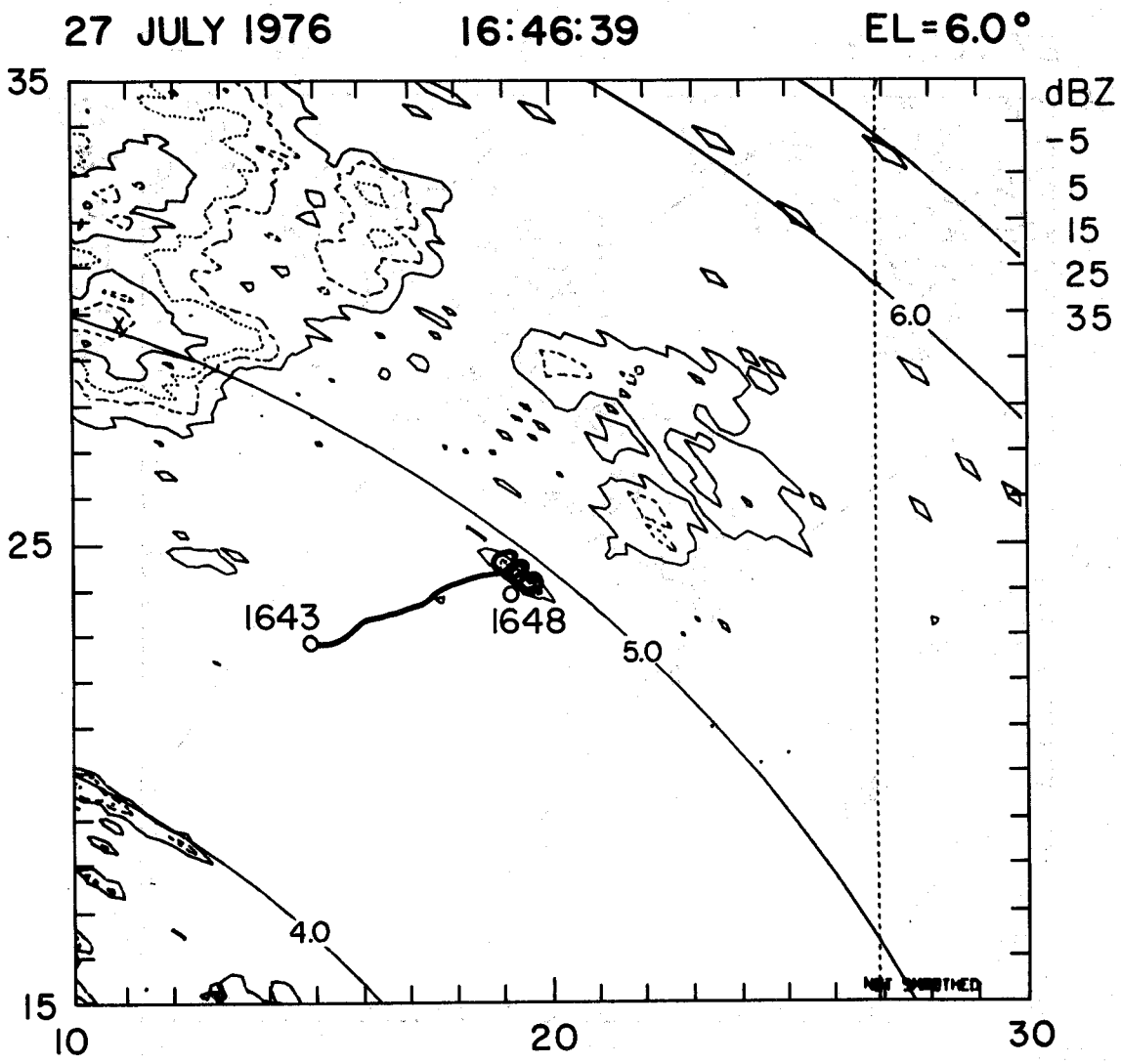

Fig. 6a. Radar reflectivities (10 dBZ contour intervals from -5 dBZ) on 20 km x 20 km PPI map at 1646:39 and 6.0° elevation angle showing sailplane track (heavy line) from 1643 to 1648. Only the endpoints of the track are marked and labeled. Constant altitude arcs are at 4.0, 5.0 and 6.0 km. Dashed line on right side is the western boundary of the dense precipitation network. Note that radar ground clutter and artifacts have not been removed from these PPI's.

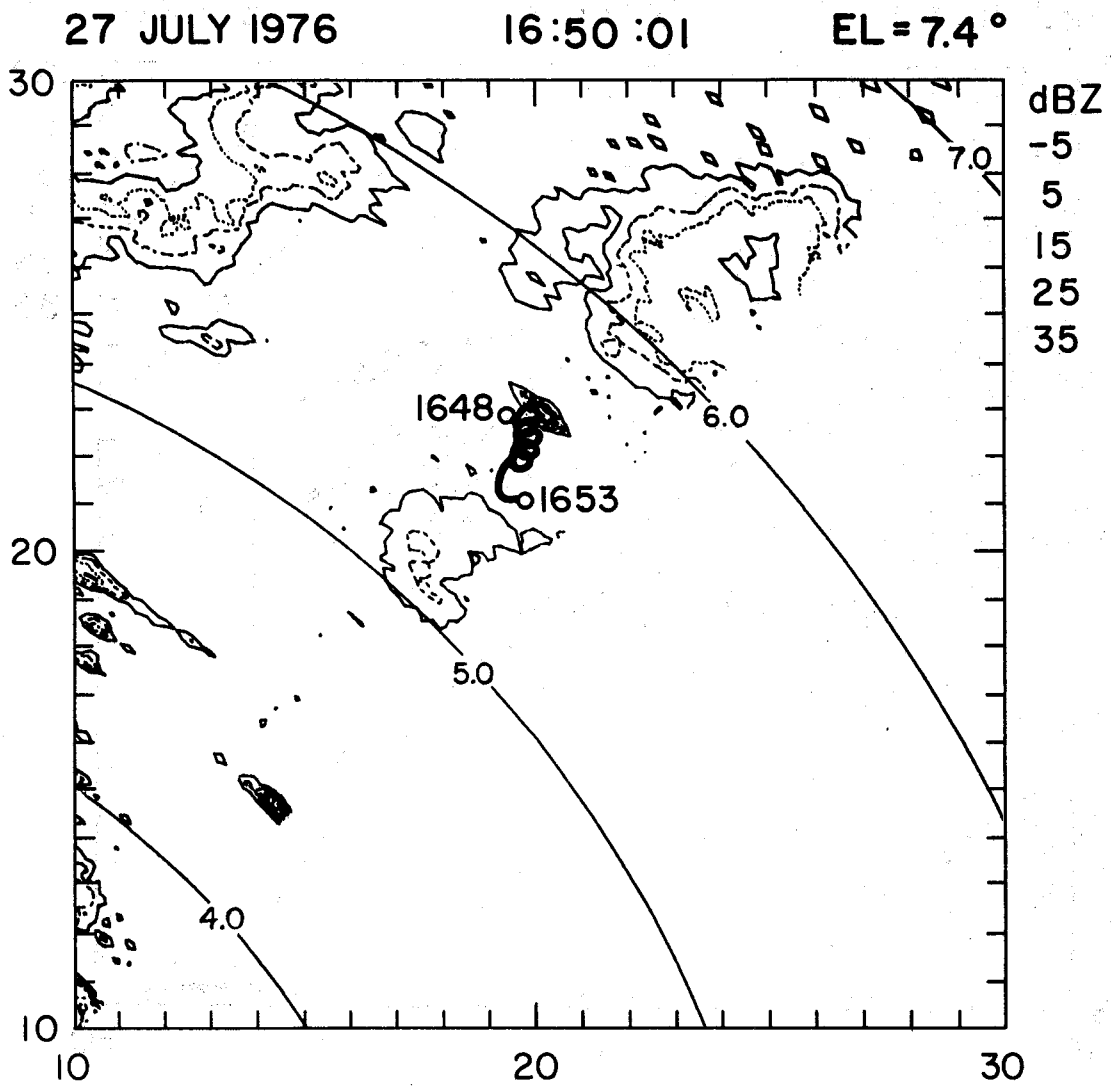

Fig. 6b. Same as 6a except PPI is at 1650:01 and 7.4° elevation angle, and track is from 1648 to 1653. Area is shifted 5 km south from Fig. 6a, and radar scan did not extend to the southeastern half of this PPI.

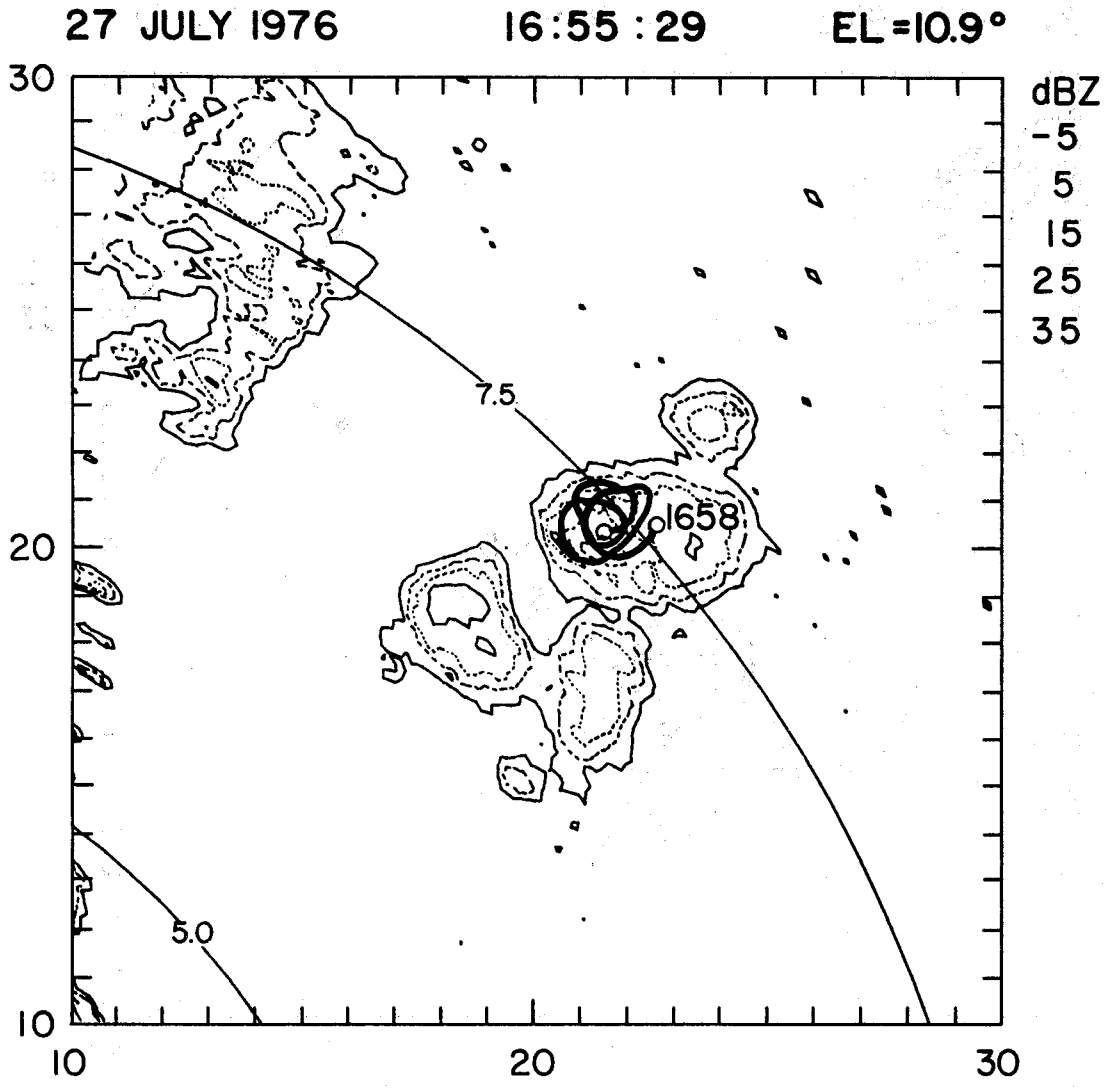

Fig. 6c. Same as 6b except PPI is at 1655:29 and 10.9° elevation angle, and track is from 1653 (not labeled) to 1658.

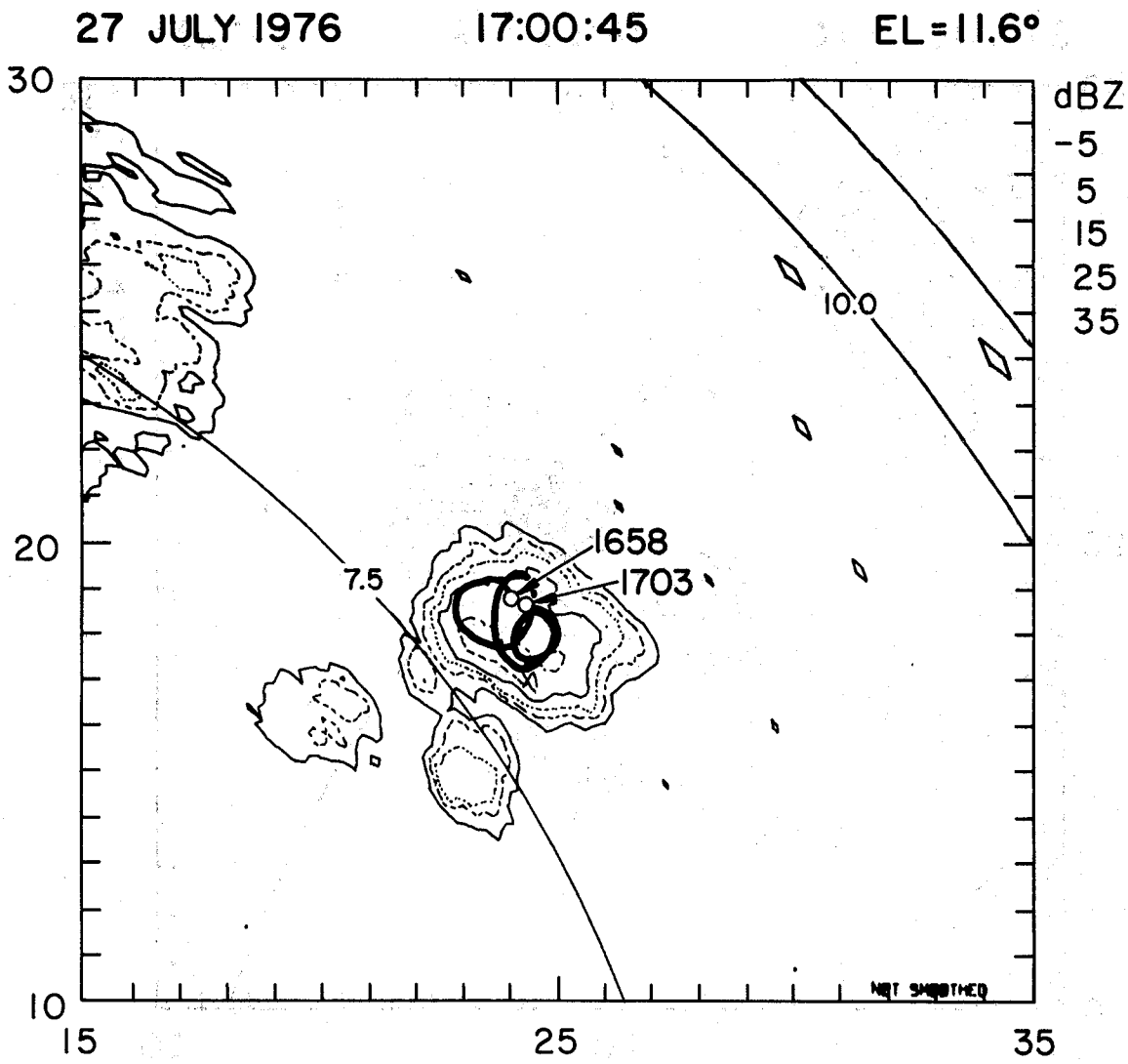

Fig. 6d. Same as 6c except PPI is at 1700:45 and 11.6° elevation angle, and track is from 1658 to 1703. Area is shifted 5 km east from Fig. 6c.

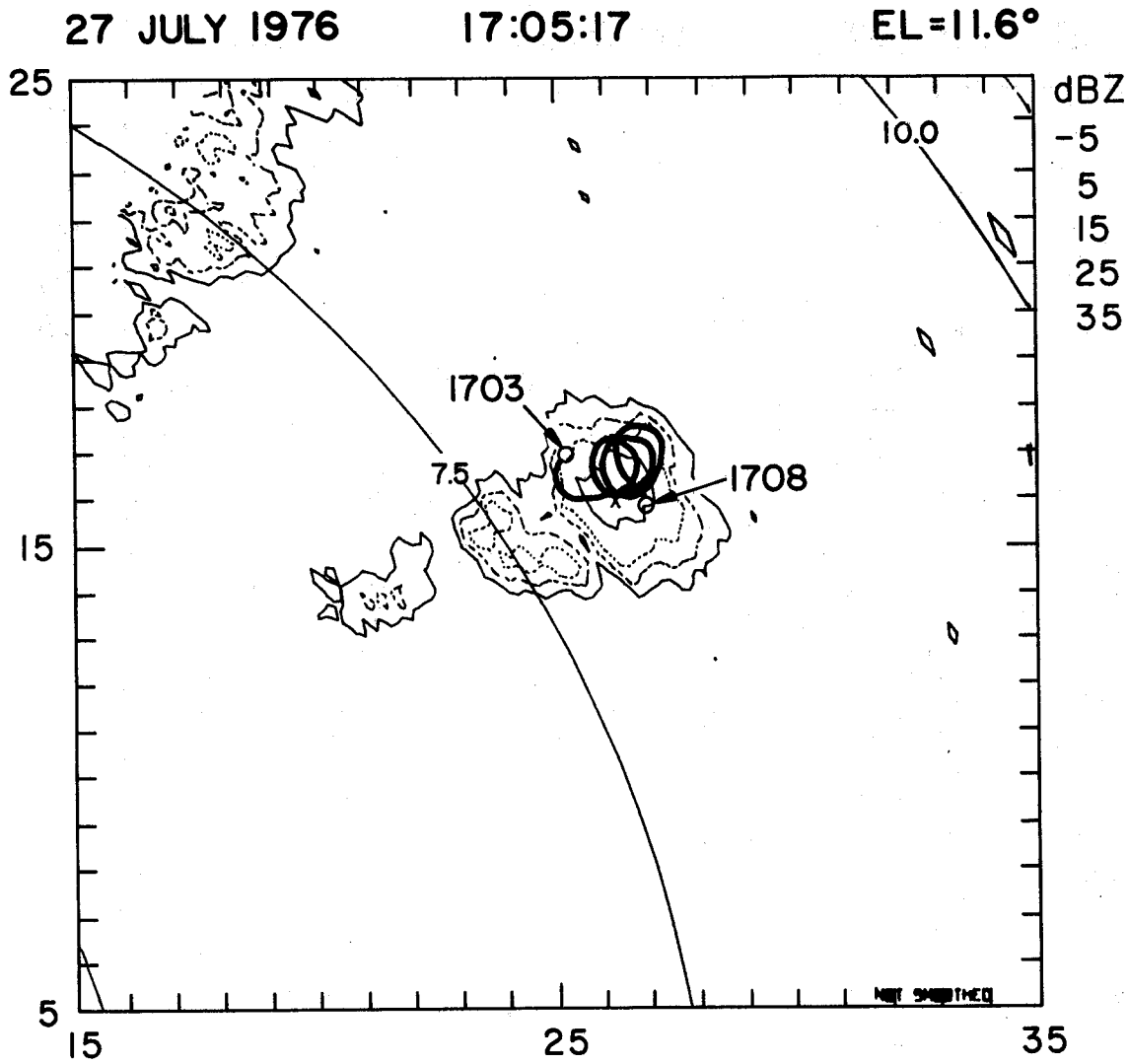

Fig. 6e. Same as 6d except PPI is at 1705:17, and track is from 1703 and 1708. Area is shifted 5 km south from Fig. 6d.

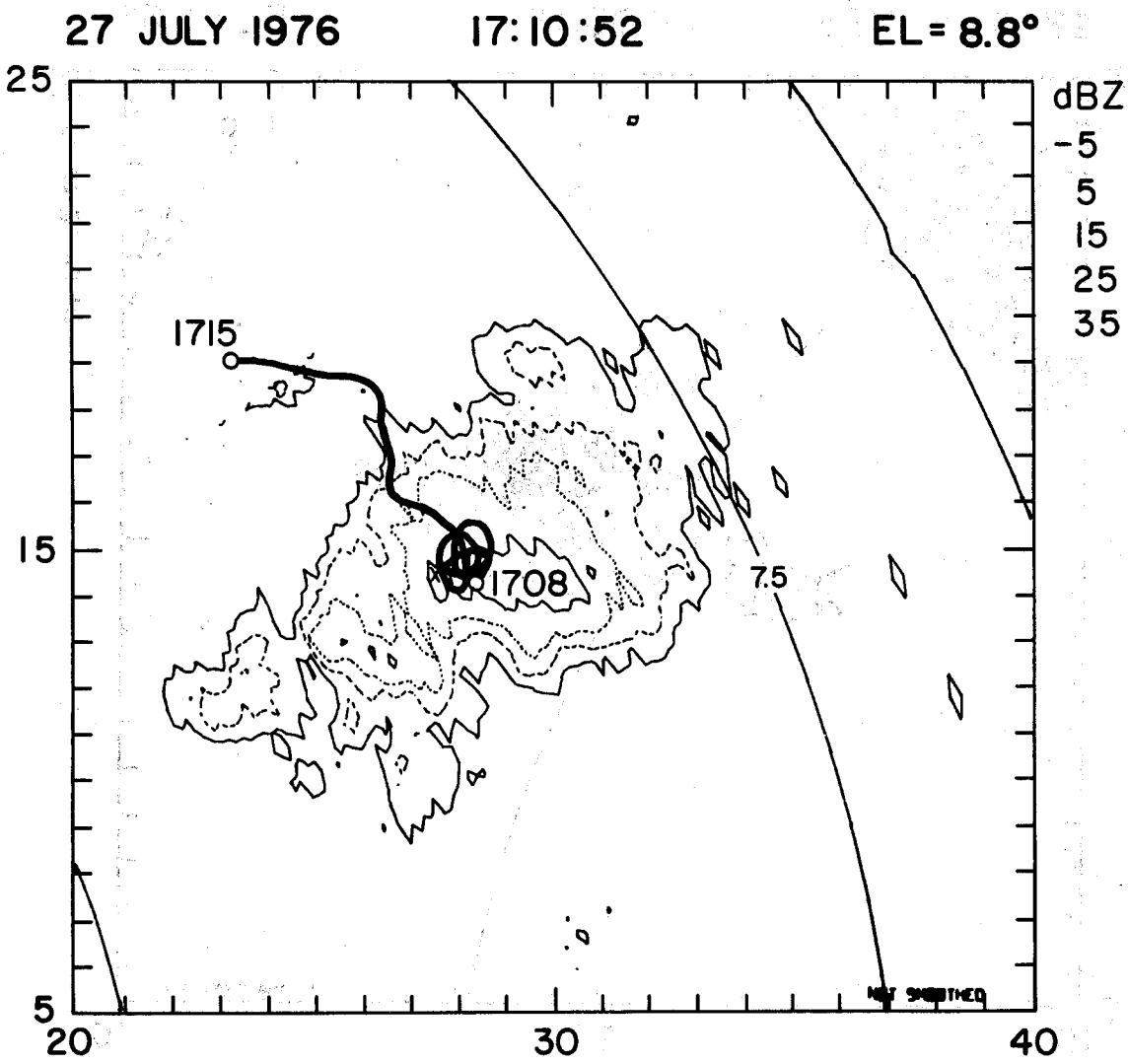

Fig. 6f. Same as 6e except PPI is at 1710:52 and 8.8° elevation angle, and track is from 1708 to 1715. Area is shifted 5 km east from Fig. 6e.

The reflectivity area which appears to be most closely affected by the updraft in which the sailplane spiralled is circled in Fig. 7, which includes three different elevation scans during the 16:56:13-16:57:34 volume sweep of the storm. The sailplane was nearing the top of its climb at this time in a strong updraft (15 m s^{-1}) with high liquid water contents (3 g m^{-3}). This reflectivity feature had fair continuity in time and space, and may be termed a "cell", although its identity became ambiguous at times. The maximum reflectivity history of the cell is presented in Fig. 8 with the sailplane's altitude history also included. After about 1712, the cell became so embedded in the storm mass that it was impossible to track as a separate entity. However, the sailplane was well positioned for following the early development of the cell. The reflectivity history shows first echo formation (-5 dBZ) at about the -15°C level, spreading upward faster than downward. Subsequent reflectivity levels first occurred at slightly higher altitudes and gradually increased their rate of descent. Upward growth ceases about 1700, which is also the time the sailplane began descending in relatively neutral air with short term peaks of updrafts and downdrafts. The downward slope of the 35 dBZ contour from 1702 to 1711 parallels the sailplane's descent and is about 4 m s^{-1}.

Altitude, temperature, vertical velocity, liquid water content (LWC) from the Johnson-Williams hot-wire device, droplet data from the PMS FSSP probe, and indications of particle images from the cloud particle camera are presented in Fig. 9 for the time period 1635-1715. The early period of the penetration is included to show the conditions initially encountered by the sailplane and to demonstrate the length

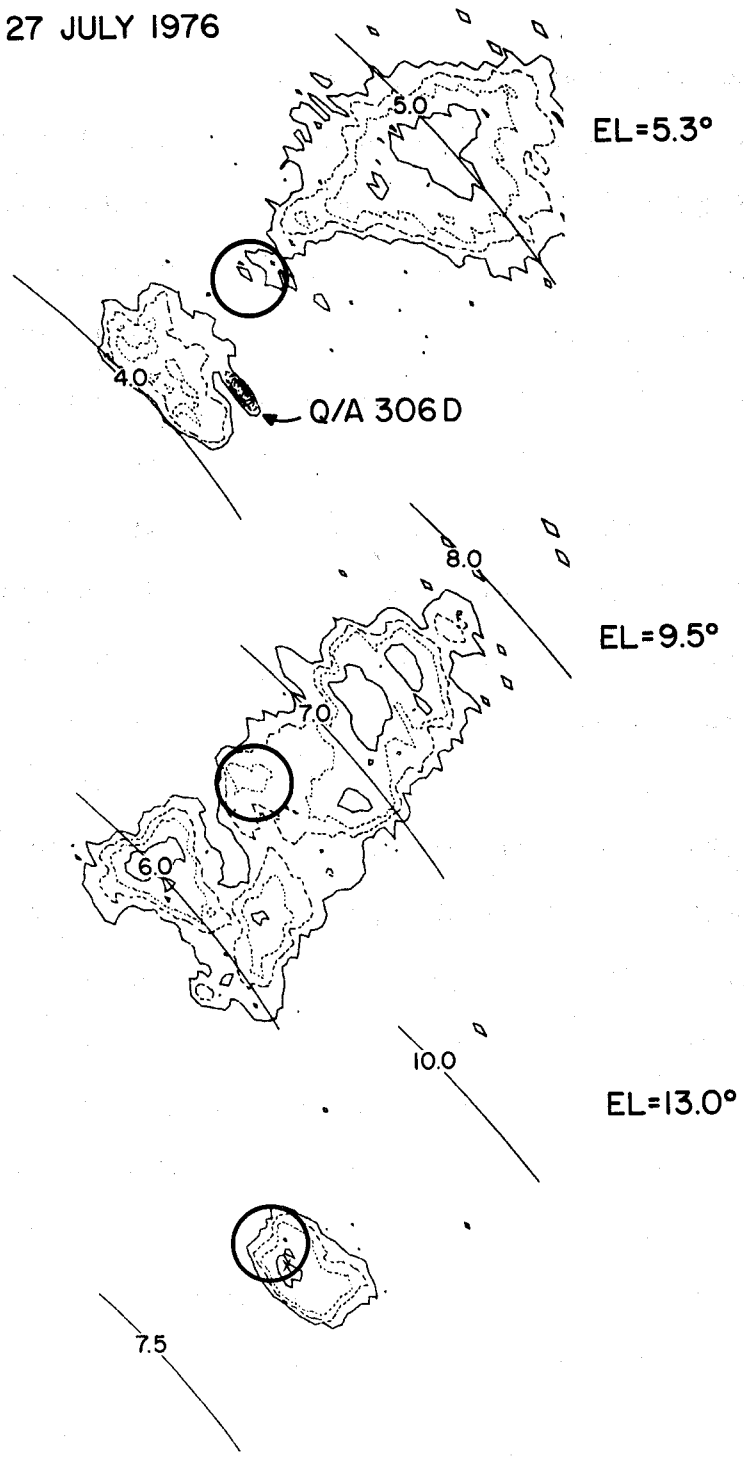

Fig. 7. Radar reflectivity (10 dBZ contours from -5 dBZ) from PPI's at 5.3°, 9.5° and 13.0° elevation angles during the 1656:13 - 1657:34 volume sweep. Constant altitude arcs are labeled for each PPI. The cell closest to the sailplane penetration is marked with a heavy circle, which is 2 km in diameter and centered at Grover coordinates (20.5, 20).

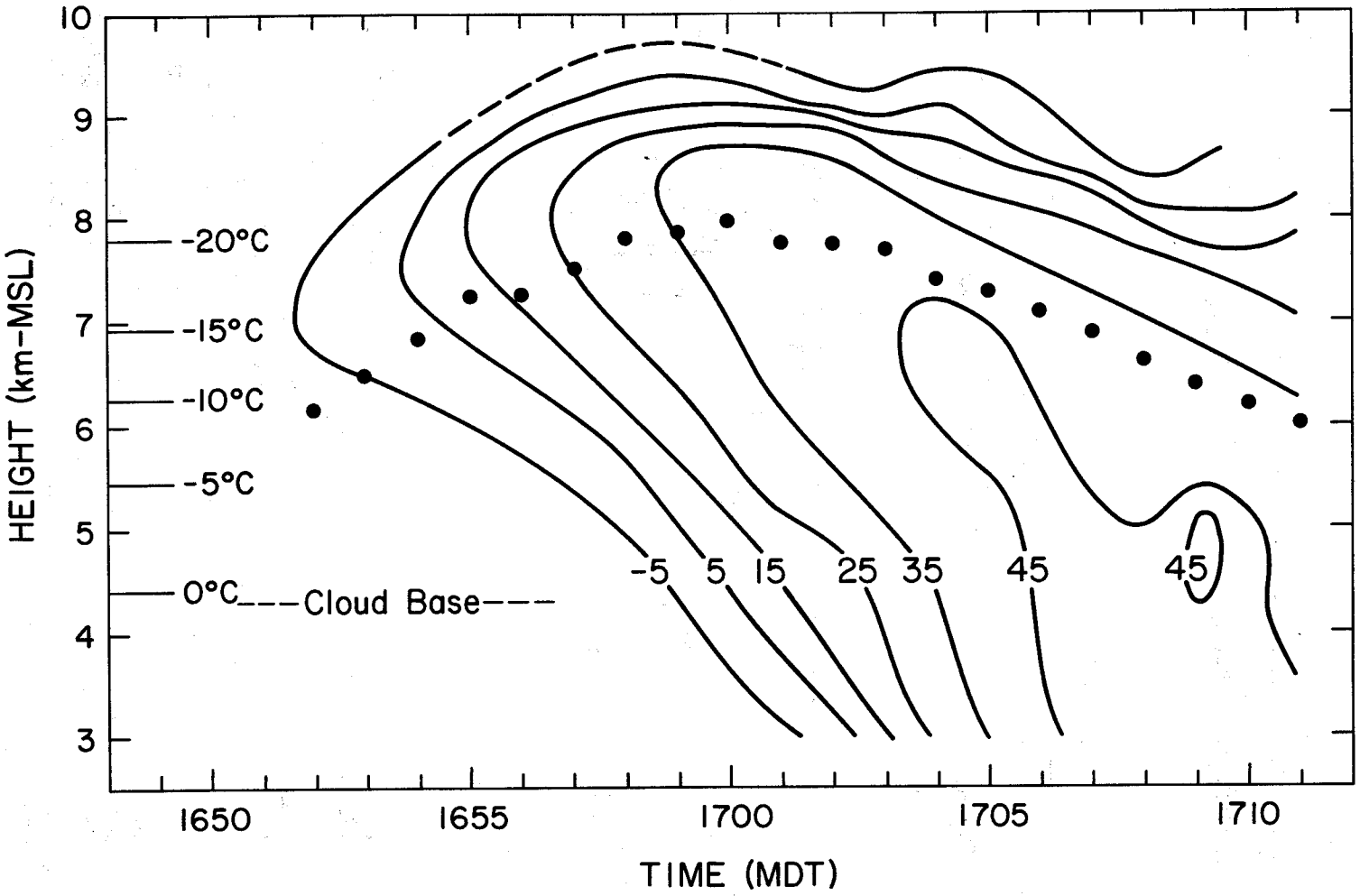

Fig. 8. Time-height profile of maximum reflectivities from the cell closest to the sailplane penetration on 27 July 1976. Contours are at 10 dBZ intervals from -5 dBZ. Dots indicate the sailplane's altitude at each minute from 1652 to 1711. In-cloud temperatures are labeled at the left (5°C intervals).

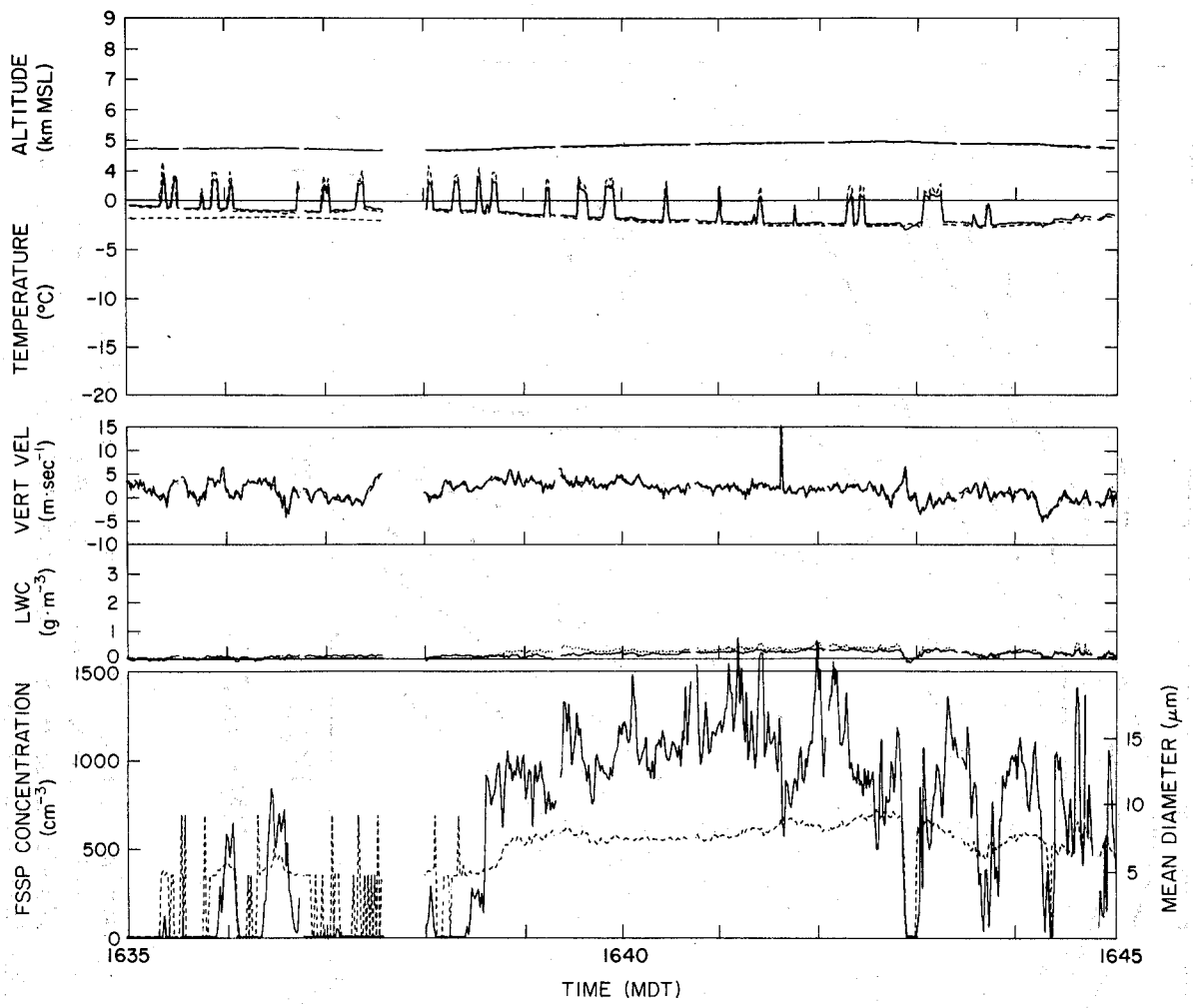

Fig. 9. Sailplane data from 1635 to 1715 showing altitude, temperature, vertical airspeed, liquid water content, and adjusted FSSP concentration and mean diameter. For altitude, the solid line is from the Hamilton Standard device and the dashed line derived from the variometer. For temperature, solid is from the reverse flow probe and dashed is from an exposed "window" probe. For LWC, solid is from J-W probe and dashed is from FSSP integrated spectra. For FSSP plots, solid is corrected total concentration with scale on the left axis and dashed is mean diameter with scale on the right axis. Times of ice particle image detection are denoted at the bottom by dots (single events) and lines (continuous events), with line thickness increasing qualitatively with ice particle concentration. See text for complete explanation of the data presentation. (Figure continued on next three pages.)

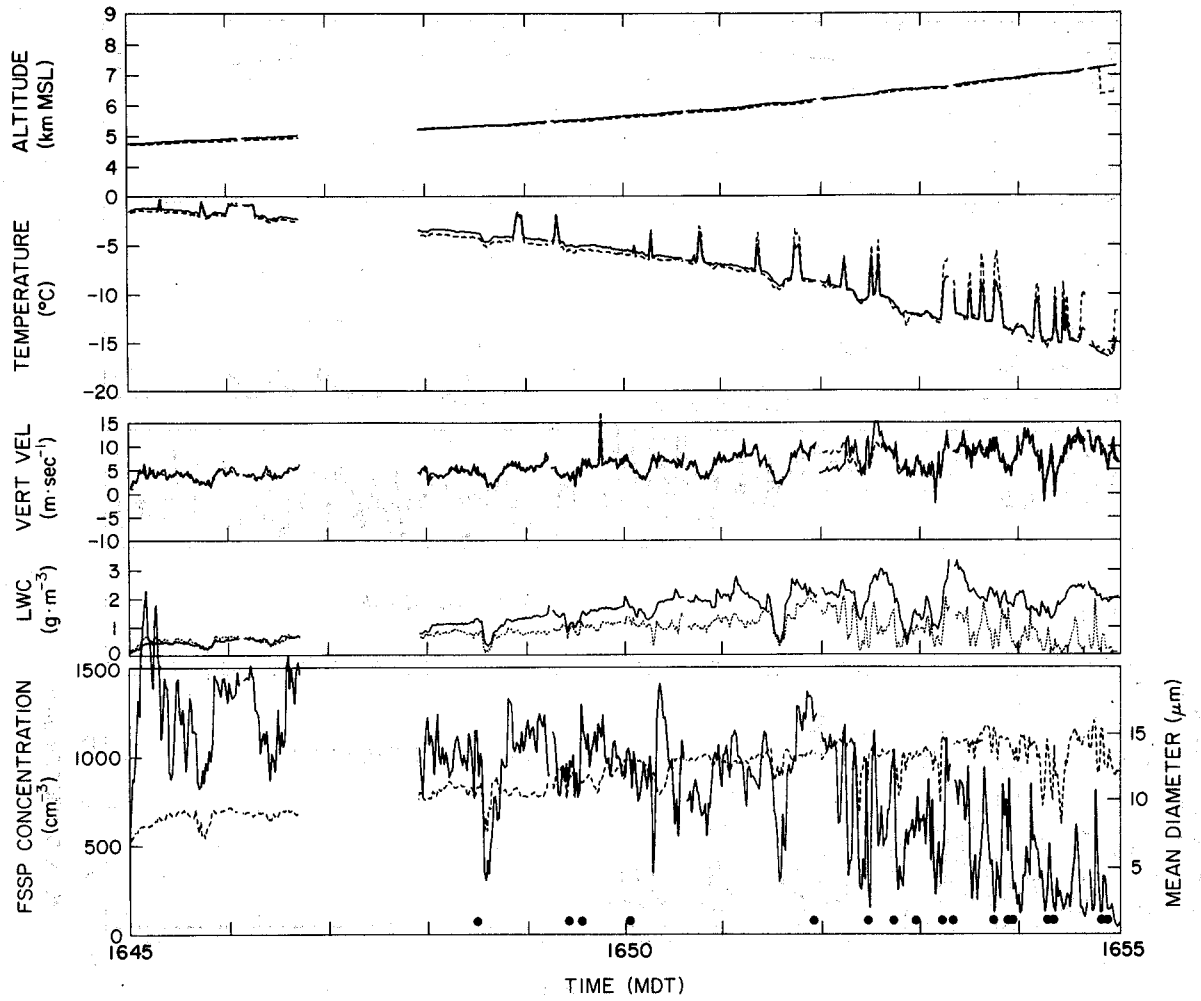

Fig. 9 (continued)

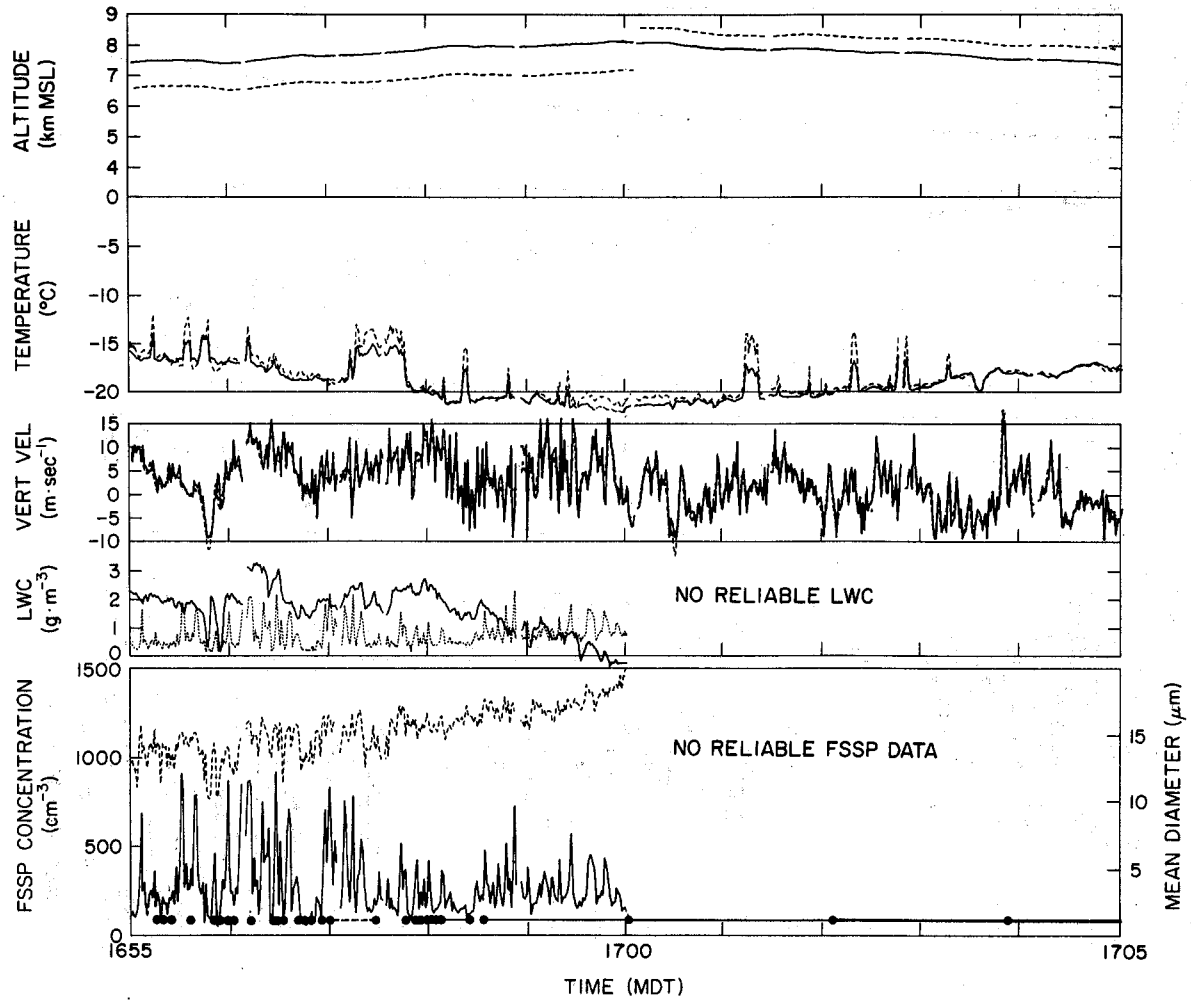

Fig. 9 (continued)

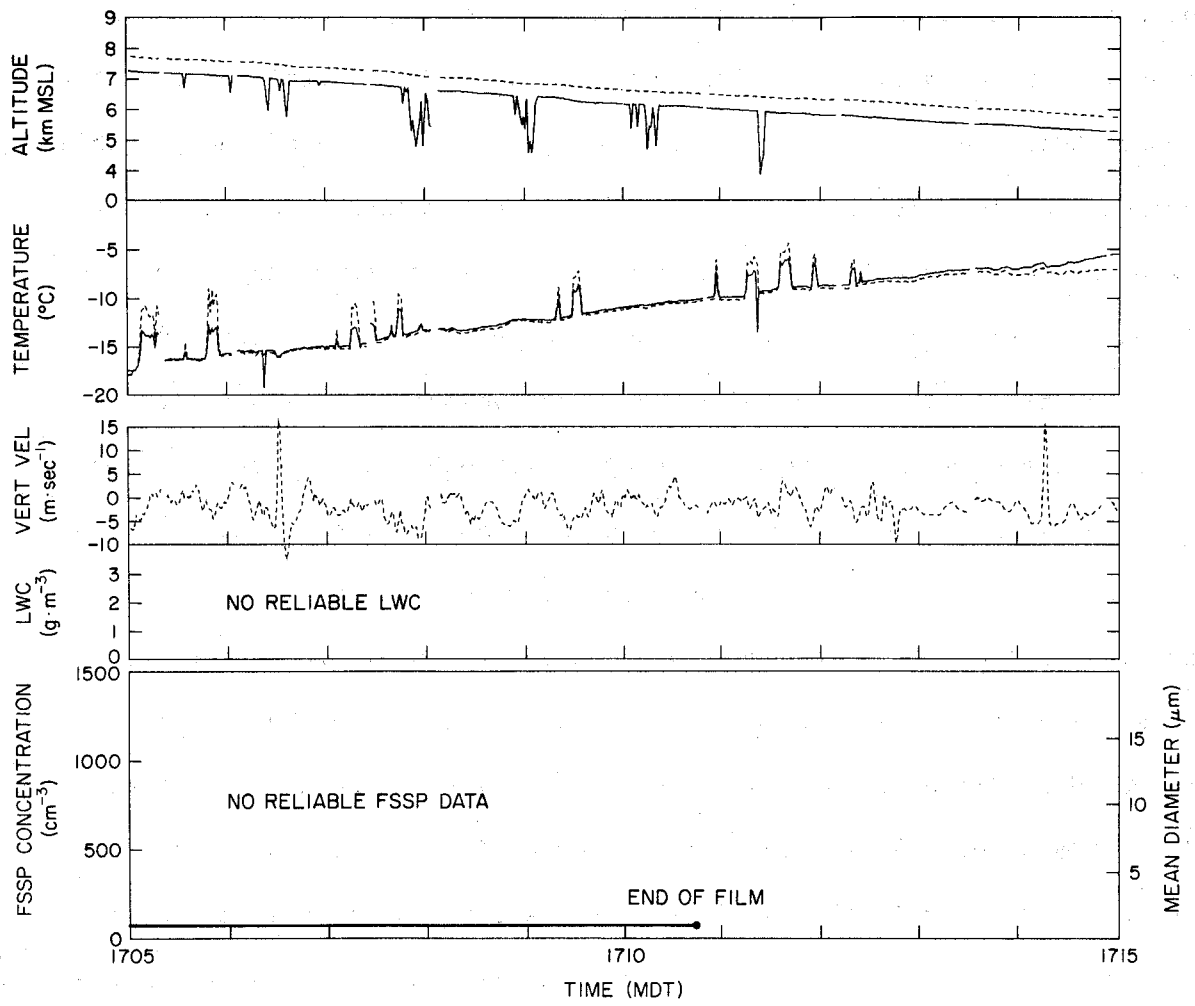

Fig. 9 (continued)

of time spent in-cloud. Bad data records caused by inadequate telemetry signals were eliminated resulting in periods of no plotted data. After about 1635, the FSSP data show signs of probe icing and of the probable presence of ice particles. The droplet concentration is decreasing and becoming more variable, the mean diameter is increasing and the calculated LWC from the FSSP measured spectrum is differing significantly from the traces of the JW LWC and vertical velocity. By 1658, other instruments show indications of icing. Although liquid water is probably being rapidly depleted due to the increase in ice particle concentration at this time, the JW LWC trace decreases too rapidly to below baseline values to be trustworthy. The dynamic pressure sensor also shows signs of icing which affects the airspeed and nearly all the computed parameters. Consequently, the quality of the data included in Fig. 9 after 1658 is degraded, and much of it becomes untrustworthy. The altitude is reliable, aside from the sharp, short-term decreases noticeable after 1705. The temperature is less accurate due to incorrect airspeed corrections, but usable to about ±1.0°C. The general trace of the vertical velocity is reasonable, but the high frequency spikes and variations are not accurate. After 1705, only the variometer-derived vertical airspeed values are presented due to the effects of the altitude fluctuations on the dz/dt calculations. The JW and FSSP probes do not give reliable data for the rest of the penetration, and their data are not included in the figure after 1700. The cloud particle camera data is unaffected except for a few brief occasions of no data due to the airspeed problem. The appendix on sailplane instrumentation provides more details of these problems.

General noteworthy features of the data are: 1) the development of the updraft as the penetration progressed; 2) the correlated increase and fluctuations of the JW LWC trace with the vertical velocity trace (until about 1658); and 3) the ice particle encounters. Between 1650 and 1658, a few small, out-of-focus images were detected by the cloud particle camera with some apparent graupel evident later in the period. Small rimed crystals and graupel of all sizes (maximum, 6.5 mm diameter) were the predominant ice forms from 1658 to about 1702 in rough concentrations of 5-15 ℓ^{-1}. During the next two minutes, the concentration increased slightly to 10-40 ℓ^{-1} and the particles were mostly graupel with some lightly rimed branched crystals. After 1704, ice particles of all kinds were present in increased concentration (50-150 ℓ^{-1}). The identifiable crystals were mostly branched and in all stages of riming, and the graupel particles ranged from <1 mm to ∿6 mm in diameter but were generally 2-4 mm.

The vertical velocity structure and development, as deduced from the sailplane data, are consistent with the simple, conceptual model of a thunderstorm cell proposed by Byers and Braham (1949). The cumulus (developing) stage spans the period when the sailplane was in a fairly strong, continuous updraft beginning at about 1645 to shortly before 1656 when the first downdraft was recorded. Downdrafts were then sampled more frequently, and the updraft encounters were not as lengthy or smooth, suggestive of the mature stage of the cell's life cycle. After ∿1705, downdrafts and generally weak conditions prevailed in the sailplane penetration, consistent with the dissipating stage of the model. The cloud particle camera data suggest that the development of

ice resulted from relatively simple particle trajectories that could be associated with the thunderstorm cell model. The first identifiable graupel particle was detected at ∿1656, which was at least 18 min but more likely 20-25 min after cloud formation. This is comparable to the result of Scott and Hobbs' (1977) microphysical model of about 14 min, although the initial cloud conditions assumed in their one-dimensional (dynamic) model differed somewhat from this case. The cloud particles photographed before ∿1656 (and sufficiently within focus to be sized) were small, and could have grown in 1 to 3 min, according to the ice crystal growth rates in the temperature range of the sample (Ryan et al., 1976). Some mixing occurred in the updraft penetrated by the sailplane since the temperature and LWC were not quite adiabatic (see Heymsfield et al., 1978). Although some ice particles may have re-circulated into the sampled updraft from older cells nearby, the strength and variation of the updraft, the temperature range of the penetration, and liquid water availability seem sufficient to account for the observed ice particle spectrum.

IV. SUBCLOUD AIRCRAFT - 306D

The NCAR Queen Air 306D investigated cloud base and subcloud conditions of the group of cells worked by the sailplane from approximately 1632 to 1704. Figures 10a-f show 306D's position mapped on the radar PPI closest to its altitude at the time of the track. Ground clutter and spurious signals have not been edited out of these PPI's The tracks have been corrected to coincide with occurrences of aircraft "skinpaint" (e.g., Fig. 10c), and have also been adjusted for a storm (cell) motion of 8 $m\,s^{-1}$ to the southeast. These corrections should give a track accuracy of about ±1 km with the largest error occurring at the track endpoints of each figure. The sailplane's position has been projected onto these figures as a stipled area to show the coordination between the aircraft. Selected parameters from 306D's data are plotted in Fig. 11 for the time period 1630-1710, and include pressure, temperature, mixing ratio, θ_e, and wind direction and speed. Computed vertical velocity is presented in Fig. 12. The limitations of these data are described in the aircraft instrumentation appendix. However, it should be noted the the vertical airspeed data are generally untrustworthy when 306D was in a turn.

A cloud base pass was made at ∿1644-1645 at which time the sailplane was directly above 306D. The measurements show cloud base to be at 595 mb with a temperature of 0°C. In the updraft at 1645-1646, mixing ratio (6.5-7.0 g kg^{-1}) and θ_e (338 K) were slightly higher than the sounding values in the mixed layer. Subsequent passes below the southeastern area of the cells detected updrafts of diminishing strength which were replaced in later passes by weak downdrafts and outflow

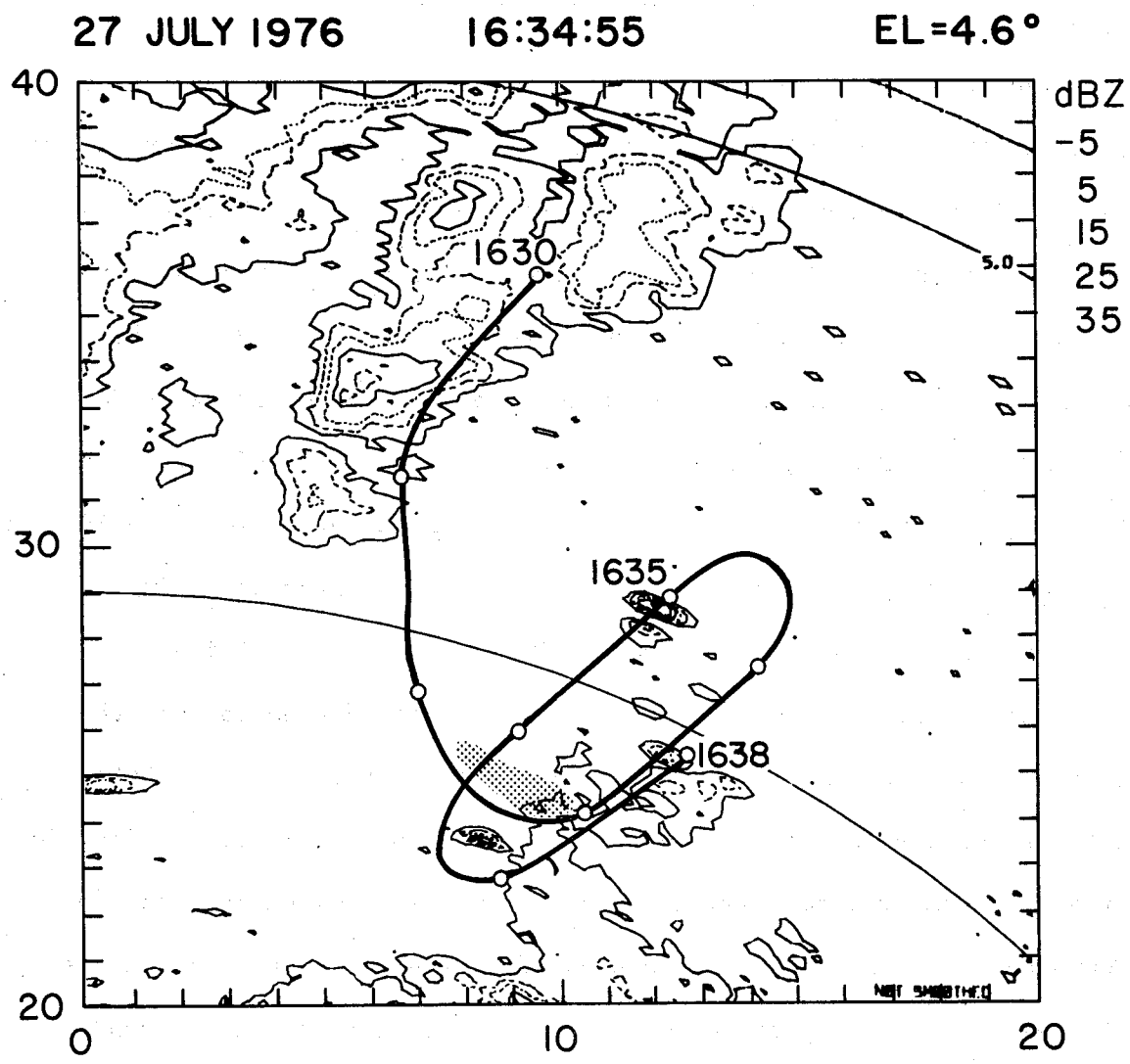

Fig. 10a. Radar reflectivities (10 dBZ contour intervals from -5 dBZ) on 20 km x 20 km PPI map at 1634:55 and 4.6° elevation angle showing Queen Air 306D track (heavy line) from 1630 to 1638. Track is marked every minute and labeled at the endpoints and one other point (1635). Constant altitude arcs are plotted at 4.0 and 5.0 km. Stipled area shows where the sailplane was operating aloft during this time period. Note that radar ground clutter and artifacts have not been removed from these PPI's.

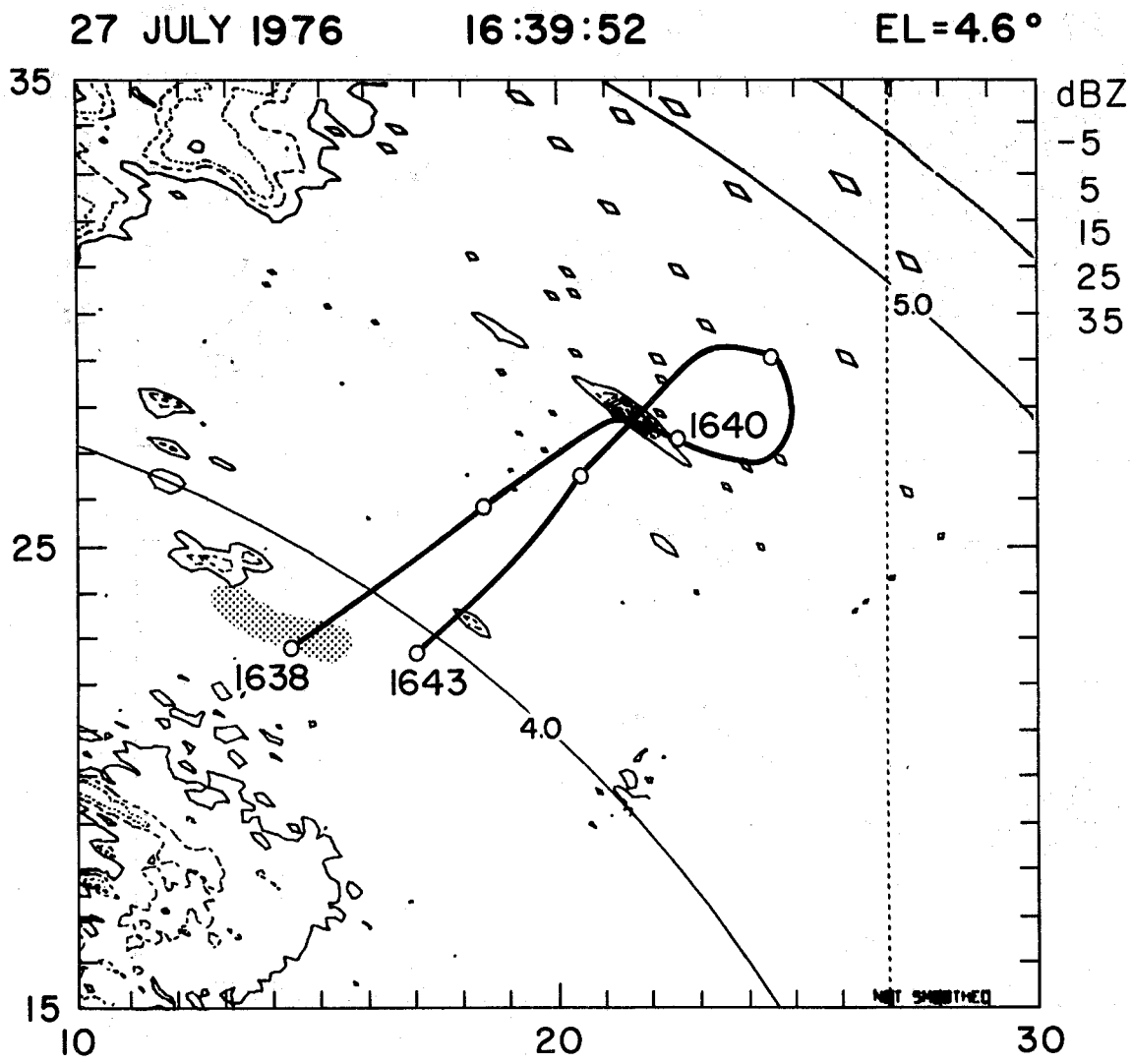

Fig. 10b. Same as 10a except PPI is at 1639:52 and track is from 1638 to 1643. Area is shifted 5 km south and 10 km east from Fig. 10a.

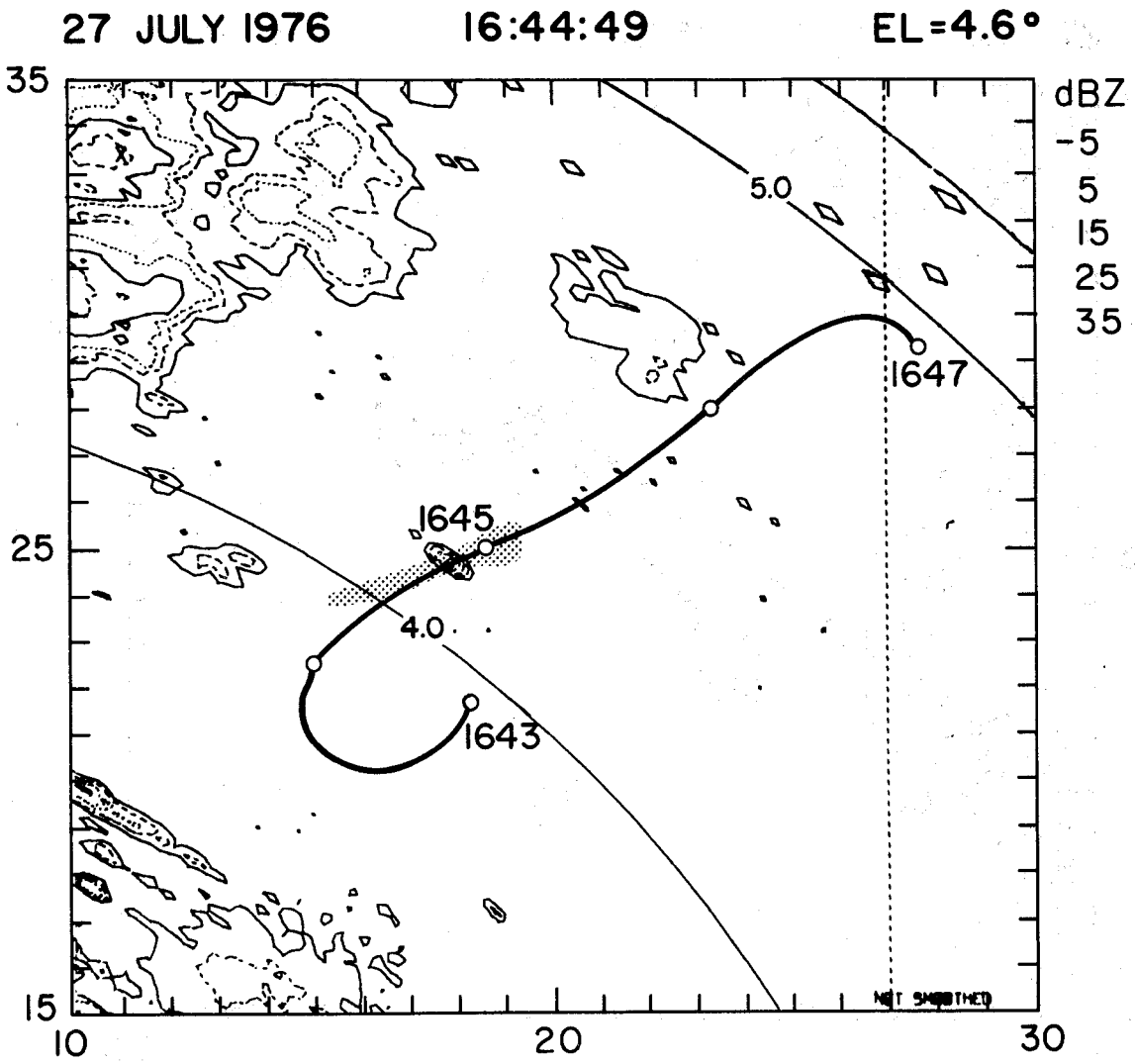

Fig. 10c. Same as 10a except PPI is at 1644:49 and track is from 1643 to 1647.

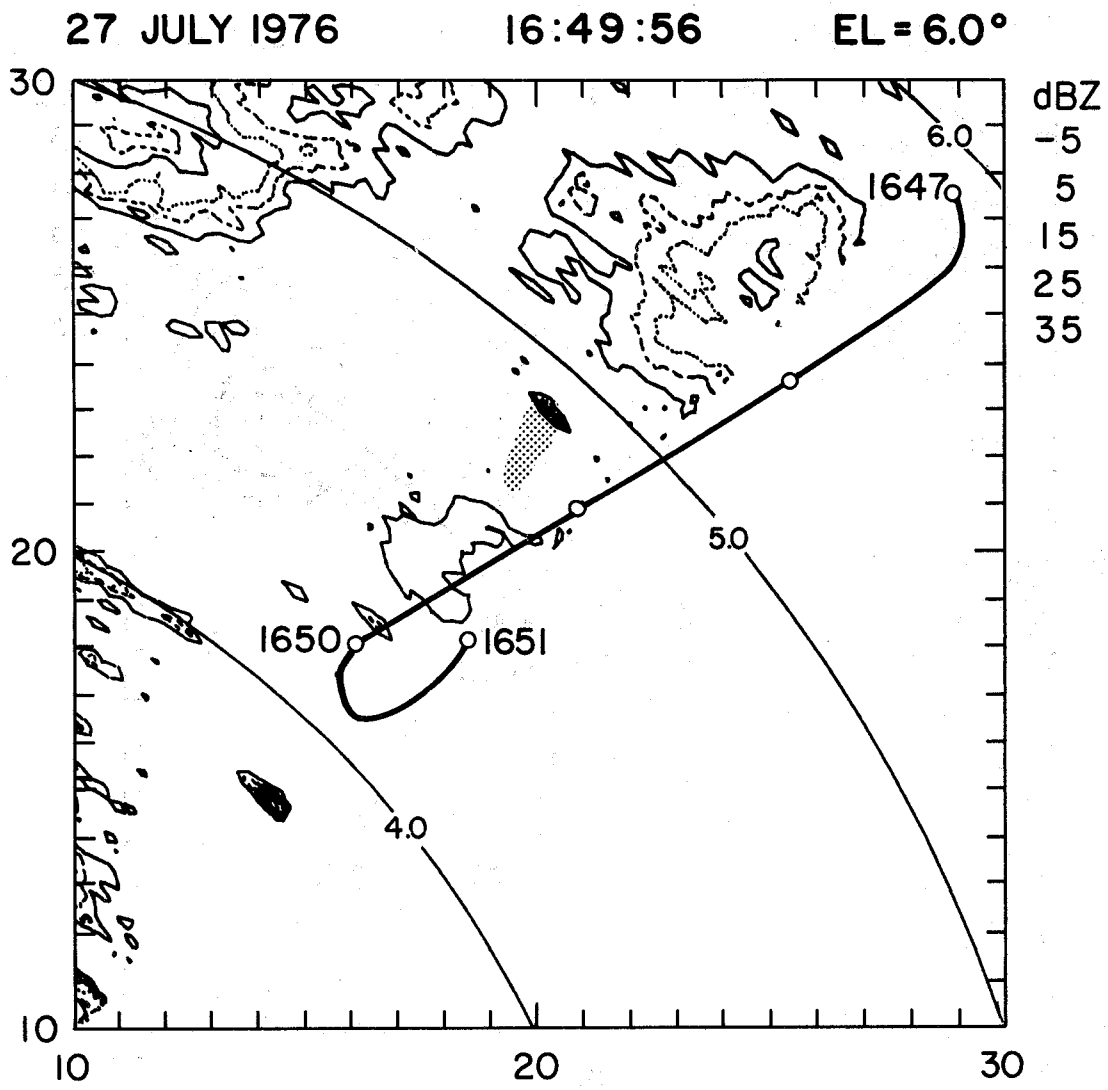

Fig. 10d. Same as 10a except PPI is at 1649:56 and 6.0° elevation angle, and track is from 1647 to 1651. Area is shifted 5 km south from Fig. 10c, and the radar scan did not extend to the southeast half of this PPI.

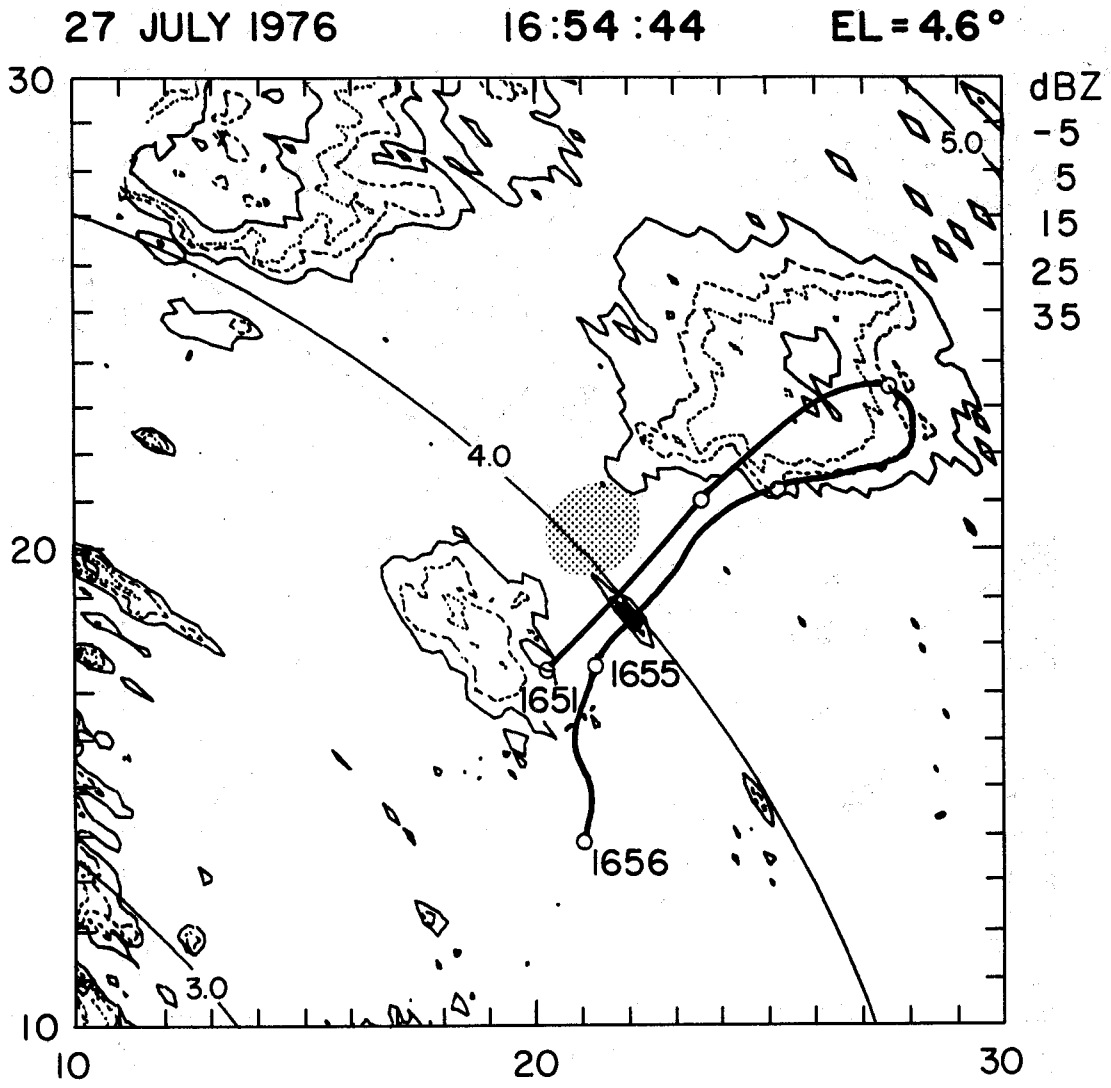

Fig. 10e. Same as 10a except PPI is at 1654:44 and track is from 1651 to 1656.

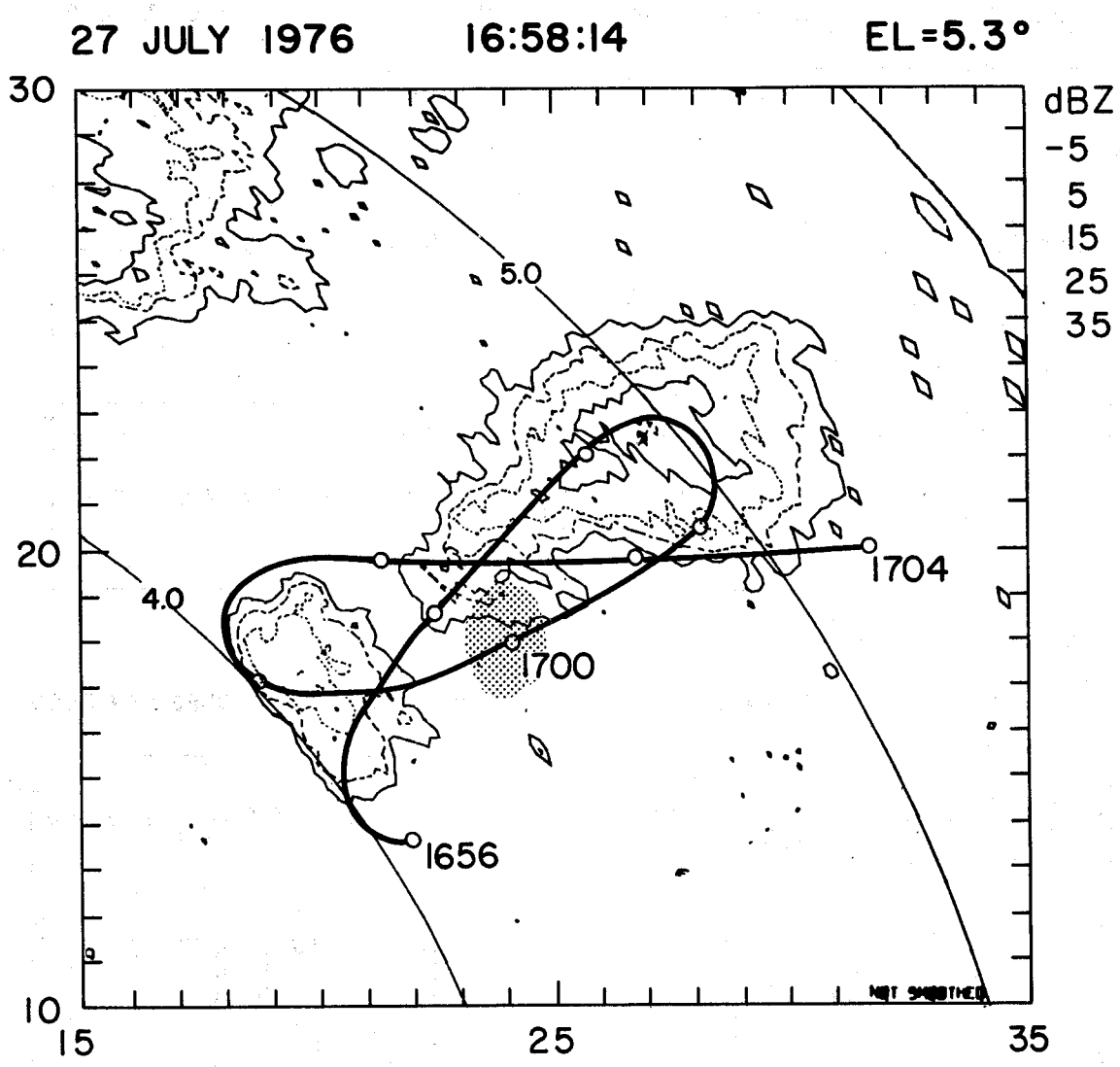

Fig. 10f. Same as 10a except PPI is at 1658:14 and 5.3° elevation angle, and track is from 1656 to 1704. Area is shifted 5 km east from Fig. 10e.

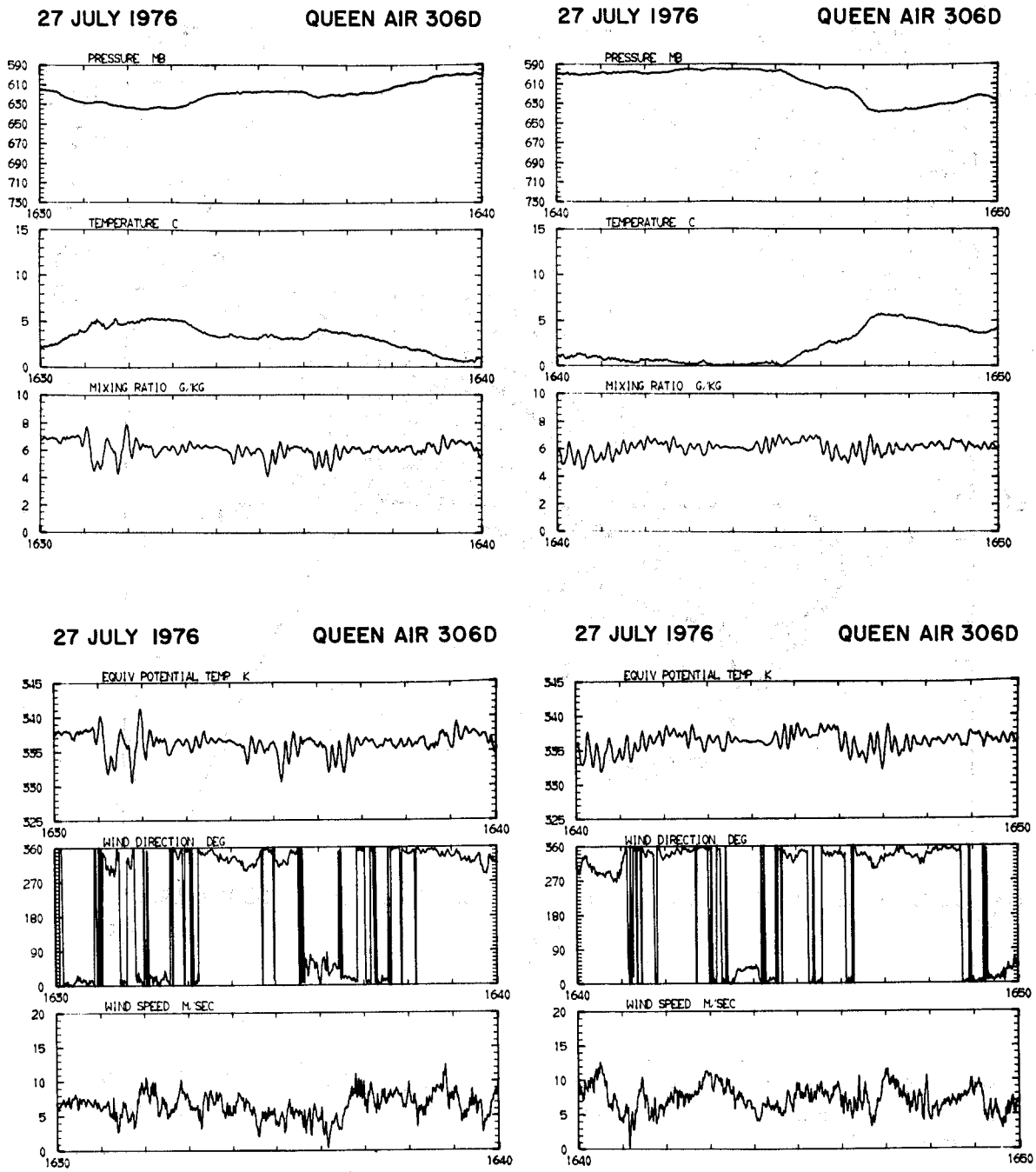

Fig. 11. Queen Air 306D data plots from 1630 to 1710 showing pressure, temperature, mixing ratio, θ_e, wind direction and speed. *(Continued on next page)*

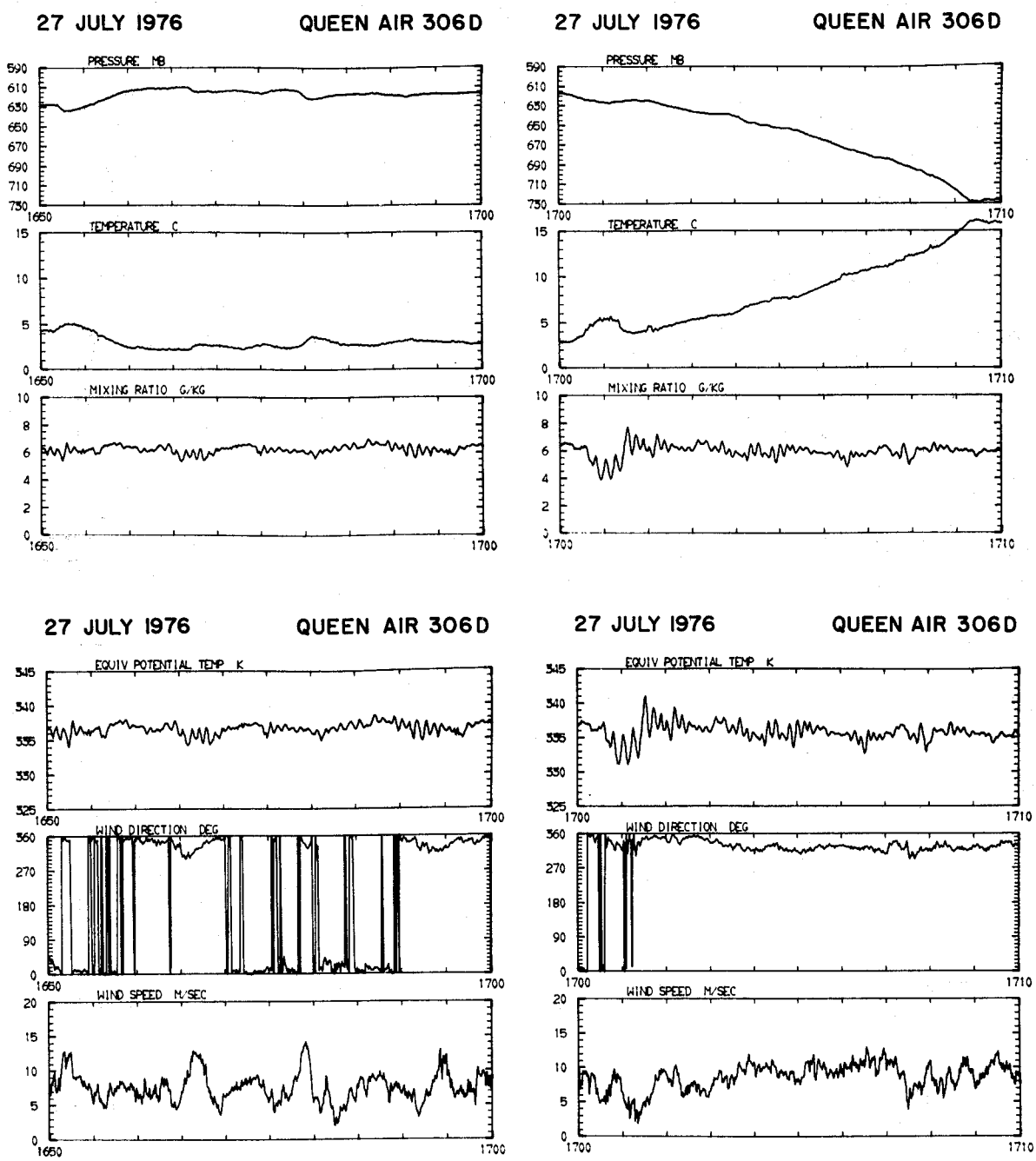

Fig. 11 (continued)

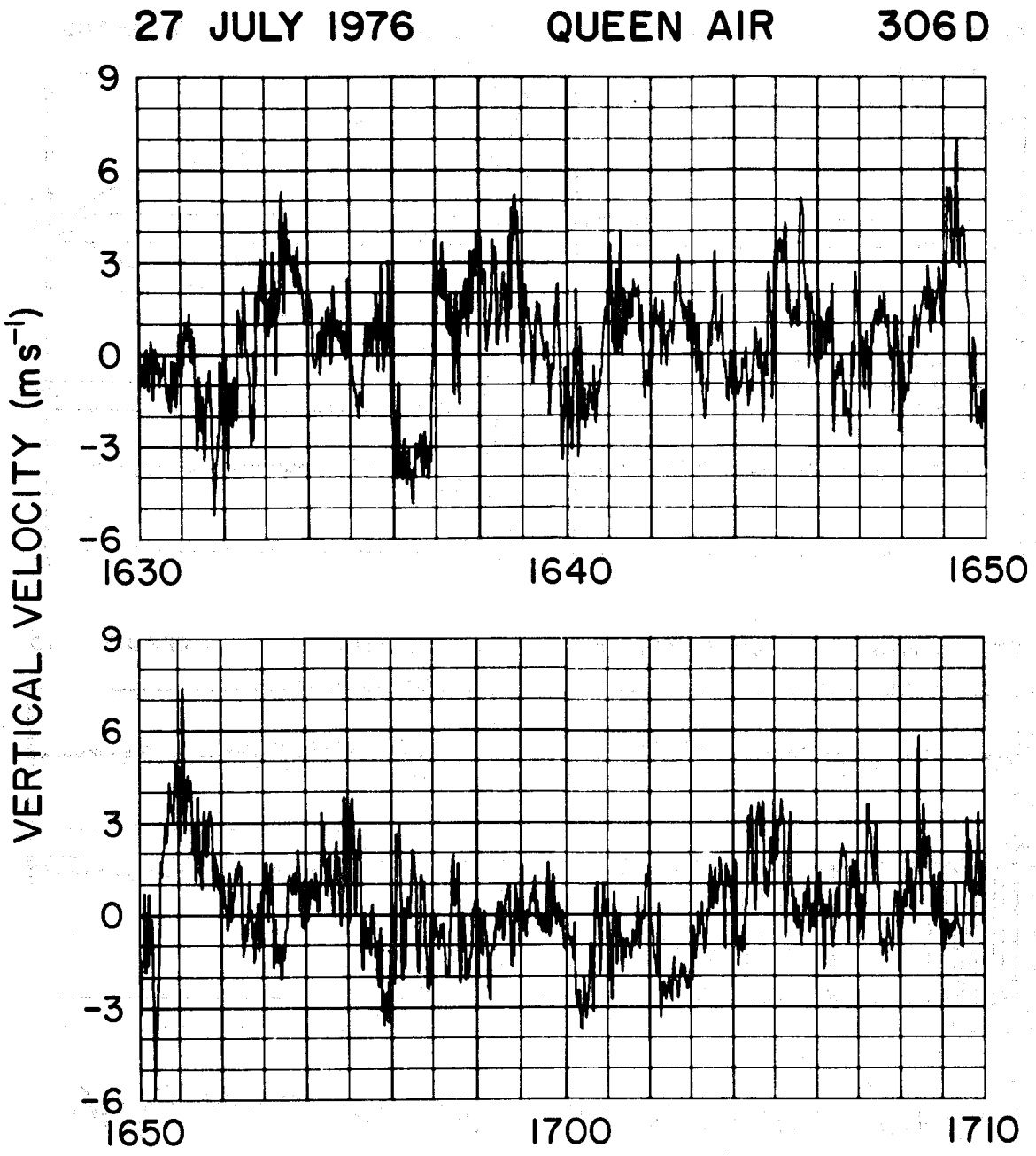

Fig. 12. Queen Air 306D computed vertical velocity from 1630 to 1710.

conditions. This was presumably due to the dissipation of the earlier developed cells of the group. The wind data show weak divergence south of the northeastern cell, with the overall winds from the northern quadrant with little or no shear, as would be expected from the sounding. Values of θ_e were generally 335-338 K with a few decreases characteristic of outfow air (e.g., at 1636-1637, 1646-1647, ∿1701).

The data from 306D's subcloud passes show weak forcing below cloud base at the time of the investigation with essentially no organization of the inflow or outflow. The cell motion was comparable to the wind through the subcloud layer suggesting that the inflow source was local below the growing cells. The passes of 306D were well coordinated with the sailplane's ascent, and the lack of a continuous cloud base updraft supports the diminished updraft the sailplane experienced at ∿1700.

V. OTHER DATA

A. Doppler Radar - Although several volume scans were made in the different areas of investigations on this day, no Doppler data were obtained for the sailplane investigation.

B. Time-Lapse Photography - Time-lapse film (16 mm) is available from five different sites on this day. They include Greeley, Lindbergh (Wyoming), Sterling, Grover, and the Butler airstrip. The quality of the film in terms of clarity and contrast is good for all the sites except Sterling where the lighting and camera setting produced poor to fair contrast on the film.

The Greeley camera took photographs of the first echo area during the sailplane penetration, but the first echo cloud was largely obscurred by intervening fair weather cumuli. There were a few brief occasions when growing turrets were visible in the vicinity of the first echo area. The Lindbergh camera was not pointed in the right direction for much of the penetration period, and when it was, the view was obscurred by the storm northwest of the first echo cloud (discussed in Section II). It was difficult to identify the sailplane-penetrated cloud in the Sterling data. Cumulus humulis to mediocris in the approximate area of the sailplane penetration were visible at the edge of the camera view area, and it is likely that the first echo cloud was either out of the view area or obscurred by other clouds. The Grover camera was redirected away from the first echo area at about 1650. Before this time, the view of the penetrated cloud was largely obscurred by near clouds although there are some frames that show a relatively clear view of growing turrets in the area of interest.

The Butler data is not useful in this study as it did not cover the first echo area. However, it captured the movement of the precipitation area from the older northwest storm as did the Grover data.

In general, the time-lapse films are not useful for any detailed analysis of the sailplane-penetrated cloud, and rarely show an unambiguous view of that area. There appears to be some useful data of other areas investigated on this day.

C. Still Photographs - Still photos were taken of the sailplane-penetrated cloud from both the towplane and the sailplane. The visual conditions of the penetration were monitored in 22 pictures taken between 1640 and 1715 by the observer in the towplane. Although the time of each photograph and the towplane's position were not accurate enough for a quantitative study, the photos provide a good visualization of the storm and put the radar structure of the storm into better perspective. The photos taken early in the period show only turrets at cloud top and portions of the surrounding cloud mass. Later, the towplane was positioned for a more complete view of the aircraft-investigated area. The photo of Fig. 13, taken 15-20 km west of the penetrated cloud at ∿1715, shows the turret investigated by the sailplane in its decaying stage. During its active period, the turret was highly visible as it rose above the surrounding clouds, but by 1715 it had collapsed and was mostly obscurred by the glaciated part of the cloud in the foreground. Maximum reflectivity at this time was about 45 dBZ in the virga below cloud base, as shown in the radar PPI of Fig. 14.

Fifteen photographs were taken by the sailplane pilot upon leaving the cloud (∿1715-1717). These pictures documented the amount of ice

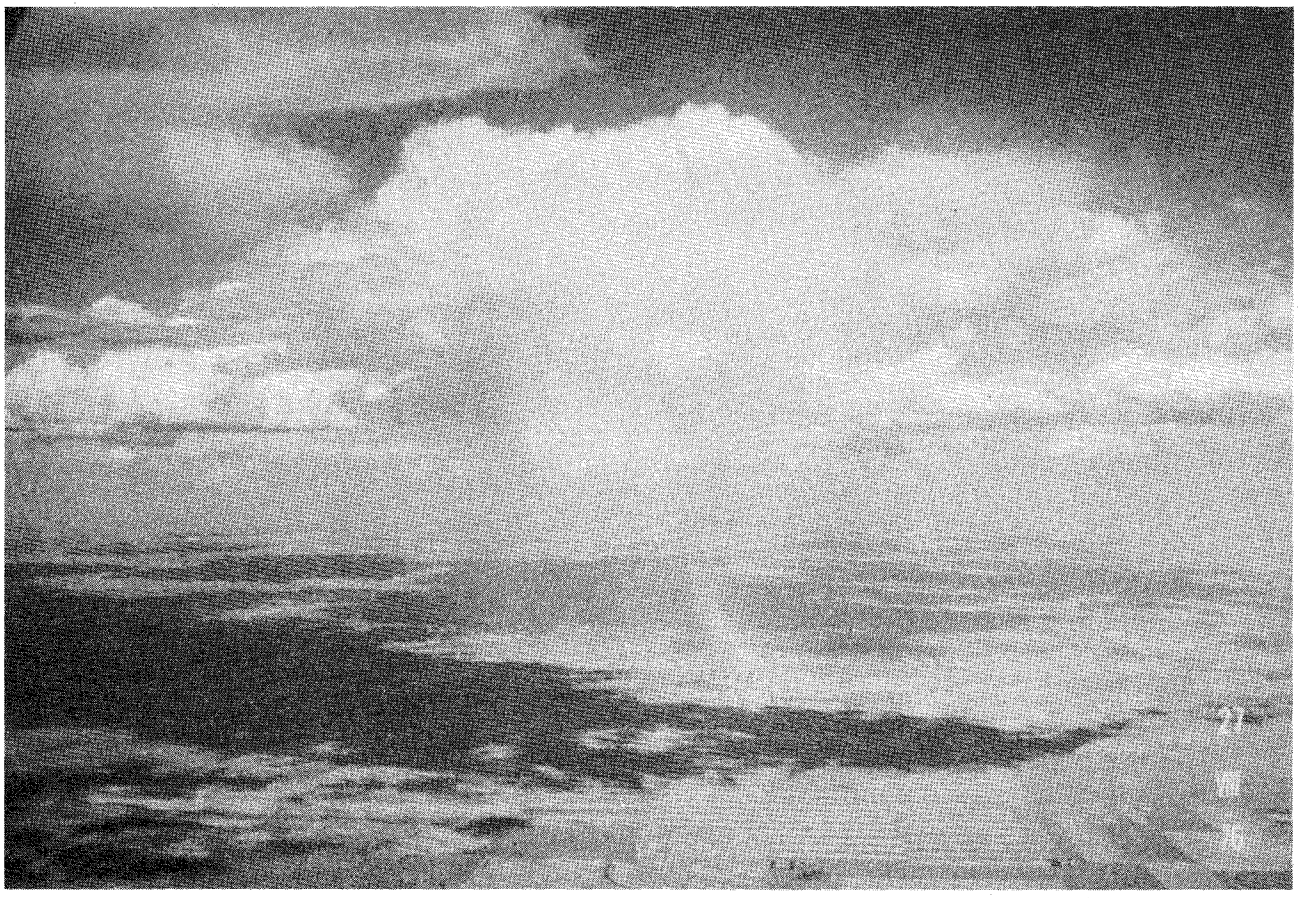

Fig. 13. Photograph of first echo storm after aircraft investigations were completed. Photo was taken from the towplane at ~1715 and 15-20 km west of the storm.

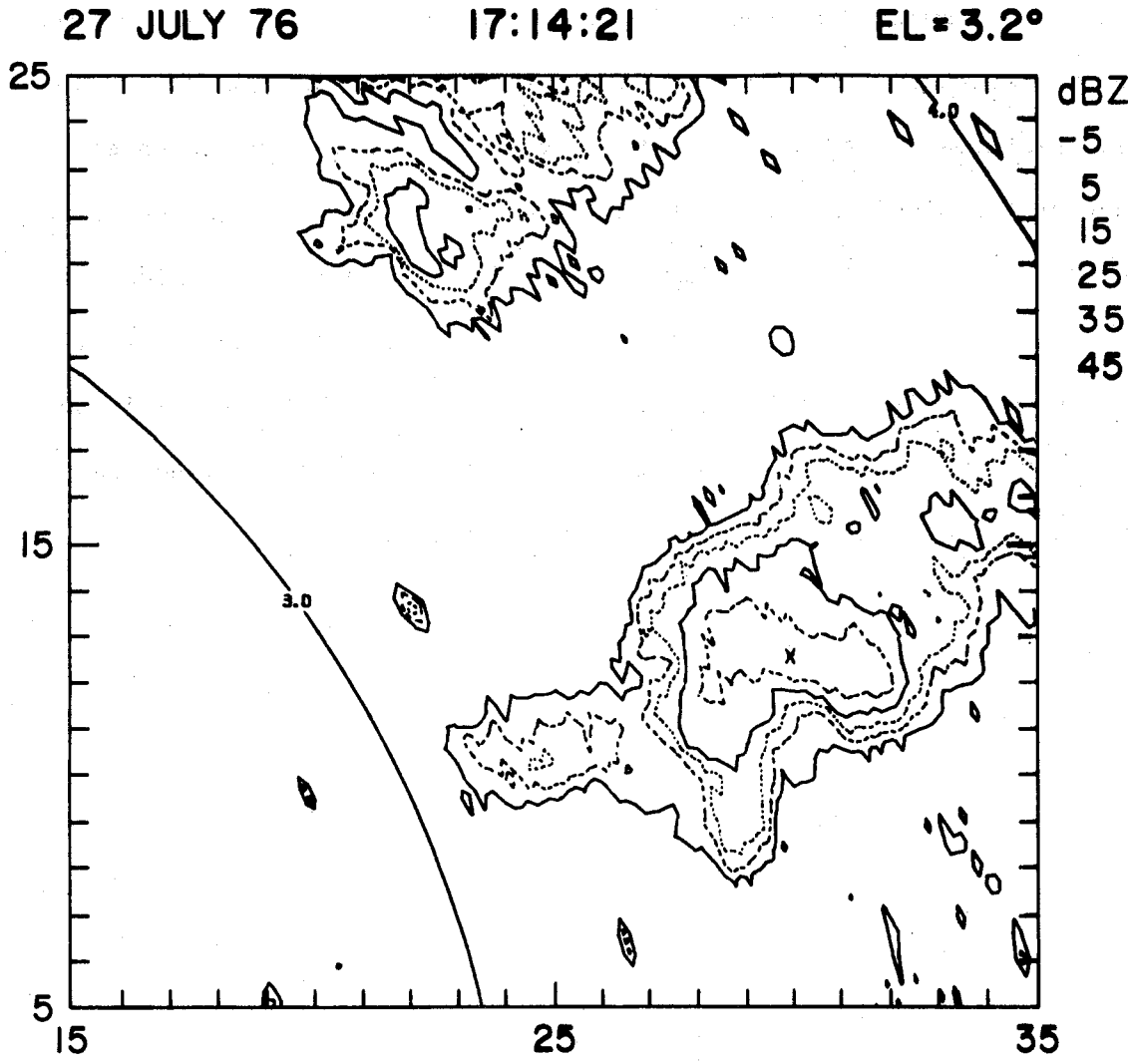

Fig. 14. Radar reflectivities (10 dBZ contour intervals from -5 dBZ) on 20 km x 20 km PPI map at 1714:21 and 3.2° elevation, about the time of the photo in Fig. 13. Constant altitude arcs are plotted at 3.0 and 4.0 km (cloud base is 4.4 km). Reflectivity artifacts have not been removed. The towplane was near the western boundary of the PPI at this time.

that had accumulated on the sailplane wings and instruments and showed the dimensions of the cloud from a closer vantage point than the tow-plane pictures. Most of the pictures viewed the north and northwest sides of the cloud as the sailplane flew out of the cloud on the north then headed west. Its position at ∿1715 is just left of the middle level clouds to the left of the glaciated area as viewed in Fig. 13. Although the sailplane is too close to capture the whole system in one photo, the extent and position of the precipitation below cloud base was well documented from the sailplane's position.

VI. SUMMARY

The 27th of July, 1976 was synoptically a weak day in the NHRE area with light winds through the troposphere, and relatively dry, stable conditions. Storms that formed were weak but lasted for lengthy periods, probably due to the lack of wind shear. The mesoscale network revealed surface convergence in the area below the investigated storm, influenced by outflow of an older storm to the northwest and by surface topography. This storm was made up of several cells that developed fairly rapidly and decayed slowly as they moved southeastward across the dense precipitation network. Very little rainfall reached the ground from this storm.

The sailplane spiralled through cloud base ($\sim$4.4 km) at about 1635 and left the cloud at about 1714 after climbing to 8.1 km and then descending 2700 m in-cloud. Though initially sampling weak updrafts, the sailplane climbed in a moderately strong and continuous updraft after moving northeast into a more active region. The ascent occurred just below the first echo level and continued in parallel with the increase in reflectivity with height (see Fig. 8). Ice particle concentration and sizes increased throughout the penetration, reaching 50-150 ℓ^{-1} with 2-4 mm graupel after the updraft had weakened near the top of the climb.

Queen Air 306D monitored cloud base conditions from 1632 to 1704 in coordination with the sailplane investigation. Inflow values of mixing ratio (6.5-7.0 g kg^{-1}) and θ_e (338 K) were slightly higher than the low level values of the sounding. There were no strong, broad

areas of inflow detected by 306D, however, and weak downdrafts and outflow conditions dominated the passes late in the period. The measured winds showed weak convergence in a few, small inflow areas but were largely from the north in agreement with the sounding measurements.

The aircraft measurements and the radar data are consistent with each other in revealing the storm's features and their magnitude. The photograph of Fig. 13 shows the storm to be small with a lot of virga, which accounts for its maximum reflectivity of ∿50 dBZ below cloud base with very little rain reaching the ground. The storm had the characteristics of a simple rainshower, similar to the thunderstorm cell described by Byers and Braham (1949), with the precipitation initiated through the ice phase process. The ice development, as detected by the cloud particle camera and suggested from the radar data, appears to be straightforward, easily explainable in terms of the model results of Scott and Hobbs (1977) and the ice crystal growth rates of Ryan et al. (1976). Although the storm is not truly isolated and dynamic effects on mixing or particle recirculation caused by adjacent cells is undetermined, they apparently do not affect the behavior of the investigated cell in a major way.

APPENDIX A

GROVER RADAR SPECIFICATIONS

The radar reflectivity data presented in the text were obtained by the Grover S-band radar (CP-2) during the 1976 field season. The specifications of the radar set are given in the table below.

Table 1. Grover S-band Radar Specifications

Antenna	
Horizontal beamwidth (deg.)	0.99
Vertical beamwidth (deg.)	0.94
Gain (dB)	44.2
Transmitter	
Frequency (MHz)	2801
Wavelength (cm)	10.7
Peak power (kw)	650
(dBm)	88.1
PRF (s^{-1})	937.5
Pulse duration (μs)	0.92
Receiver (logarithmic)	
Minimum detectable signal (dBm)	-107.4

In calculating Z_e (effective reflectivity) from the radar equation for meteorological targets, $|K|^2$ was set equal to 0.93, which is the value for water targets. ($|K|^2$ is related to the complex index of refraction of the target.) The CP-2 radar has an unambiguous range of 160 km.

In this and preceding technical notes (22 June 1976, 22 July 1976, and 8 June 1976), the radar PPI's were plotted with an azimuth angle error. From 23 July 1975 to 2 July 1976, the azimuth angle is in error by 1.03°. The error is 0.83° for the rest of the 1976 field season radar data. Aircraft tracks in these technical notes are correct in relation to the radar echoes, but absolute coordinates (from Grover) will be slightly in error due to the azimuth errors. Subsequent technical notes will incorporate the azimuth corrections into their PPI presentations.

Methods used for calibration of the radar and more detailed information about the radar are described in Foote et al. (1976) and Eccles (1975).

APPENDIX B

SAILPLANE INSTRUMENTATION

The meteorological parameters of interest measured or calculated from measurements by the NCAR/NOAA sailplane are pressure altitude, vertical airspeed, temperature, liquid water content, cloud droplet spectrum and precipitation particle concentration and type. Data are sampled every second and recorded on magnetic tape at a ground station via FM telemetry from the sailplane. True airspeed is generally about 40 m sec^{-1} and bank angle in the spiral flight mode is roughly 15 to 30°.

Pressure Altitude

A Hamilton Standard pressure transducer is used to measure pressure, which is then reduced to altitude using a nearby sounding. Accuracy is about ±10 m. The resolution, which is important in the calculation of vertical airspeed, is 0.5 m. Electronic noise occasionally interrupts a timing circuit directly involved in the measure of pressure. When this happens, the altitude always deviates to lower values, and these temporary drops are quite apparent on the altitude plot of the sailplane data.

A variometer is also used to determine pressure altitude by summing rates of change with time and adding the resultant height to the initial altitude of the sailplane. Although the response time of this instrument is slower than that of the Hamilton Standard device, agreement between the two is usually very good. Errors, brought about by

sharp gradients of updrafts or downdrafts or other flight phenomena that are not adequately measured by the variometer, are cumulative, with the result that the altitude measured in this way can drift to 500 m in 10 min.

Vertical Airspeed

The equation for calculating vertical airspeed (see Dye and Toutenhoofd, 1973) is:

$$w = \frac{dz}{dt} + \frac{|\vec{v}|D}{mg} + \frac{1}{2g}\frac{d}{dt}\left(|\vec{v}|^2\right) \quad ,$$

where w is the vertical airspeed, t the time, $\vec{v}$ the sailplane velocity, D the drag force on the sailplane, m the mass of the sailplane and g the acceleration due to gravity. Assumptions include hydrostatic equilibrium of the atmosphere, no side slip of the sailplane and no abrupt flight maneuvers. Also, vertical speed induced by horizontal wind changes is ignored. In other words, it is assumed that the horizontal wind is steady, or that over a few seconds, small-scale fluctuations average out to zero. Uncertainty from this calculation when the sailplane is spiralling in clouds is about 2 m sec^{-1}. The most important variables are rate of change of altitude and true airspeed. Minor variables are temperature, pressure, bank angle, angle of attack, and indicated airspeed which are used to derive the true airspeed and the sailplane's drag force. Significant errors in vertical airspeed are caused by errors in the major input parameters. True airspeed can be lost altogether due to icing of the pitot tube, or false altitude changes can be caused by the deviations in the Hamilton Standard derived

altitude mentioned above. Vertical airspeed can be calculated using the Hamilton Standard derived $\frac{dz}{dt}$ or using the dz/dt determined directly by the variometer. Usually the vertical airspeed plots derived by the two methods are nearly identical.

Temperature

Air temperature is measured by a reverse flow temperature probe, designed for the slow flight speeds of the sailplane. Discussion of the calibration and intercomparison of this probe with other sources is presented in Heymsfield et al. (1978). Wetting of the sensing diode when in cloud does not appear to occur with the sailplane probe, and the stated accuracy of ±0.5°C appears to be correct. Another source of air temperature data is collected by a "window" probe, and is usually plotted with the reverse flow temperature. The "window" probe is an identical sensing diode exposed to the airstream in a vent located in the nose of the sailplane. The accuracy of the diode is also ±0.5°C but it inherently becomes wetted or iced during cloud penetrations.

There is one significant problem with the temperature data. When the communications radio is transmitting, RF noise influences the voltage drop across the diode, thereby causing increased temperature readings. This noise is evident in other (minor) data channels as well as in the sharp changes in the temperature plot, and is easily identified. It has not been edited out of the data plots presented in the text.

Liquid Water Content

A Johnson-Williams hot-wire device is used for measuring liquid water content (LWC). Calibration and comparison discussions are presented in Heymsfield et al. (1978). Best estimates suggest an accuracy within ±20%. However, when the sailplane encounters high liquid water contents in supercooled conditions for extended periods, the probe's strut accumulates enough ice apparently to interfere with the flow to the sensor. This is usually identifiable by the "spikey" appearance of the J-W LWC trace, which has also become uncorrelated with the vertical airspeed trace. This condition occurs only when the high liquid water conditions have existed for roughly 10-15 minutes.

The FSSP (described below) integrated cloud droplet spectrum also provides a measure of LWC, and is plotted with the J-W output.

Cloud Droplet Spectrum

A Particle Measuring Systems (PMS) forward scattering spectrometer probe (FSSP), mounted on the sailplane, measures cloud droplet spectra. This probe, reported in various articles (for example see Knollenberg, 1976), sizes particles 2-30 μm in diameter with a suggested error of ±10% or ±2 μm, whichever is greater. Concentration accuracy had not been determined, and comparison with the J-W LWC, vertical airspeed, and different flight conditions suggested that the FSSP on the sailplane was measuring concentrations lower than would be expected.

Investigation of the probe's electronic design by personnel at the University of Wyoming revealed that coincidence errors, coupled with a retriggerable electronic delay (which allows time for the electronics to

size and count pulses), results in a greatly reduced measured droplet concentration in comparison to the true concentration. Assuming that the time between individual droplets can be described by a Poisson distribution, Dr. W. A. Cooper of the University of Wyoming has shown that the equation,

$$N_m = N_o \exp\left(-uA\tau N_o\right) ,$$

can be used to determine the measured concentration (N_m) from the true concentration (N_o), where u is the true airspeed, A the total sampling area, and τ the delay time. For the sailplane FSSP and the range of droplet concentrations found in northeastern Colorado, N_m is a monotonic function of N_o. However, for the University of Wyoming's Queen Air N10UW, N_m is bi-valued with the maximum at $\sim$500 droplets cm^{-3}. For the South Dakota School of Mines and Technology's armored T-28, the plateau value is about 200 cm^{-3} measured concentration.

The FSSP data presented in the text have been corrected using the above equation and the best determinable values for A and τ.

Ice particles passing through the sample area apparently give multiple, specular reflections which are measured by the FSSP as individual particles. In regions where considerable ice particles are present, this artifact is most noticeable as a spectrum tail in the larger channels and invalidates any measurements in the largest 7 or 8 channels as well as the calculated droplet dispersion. The counts in these regions should not be used as a measure of the ice particle concentration, since one ice particle apparently gives rise to more than one apparent droplet count.

An added problem with the FSSP data arises due to icing of the probe. After only a few minutes of in-cloud sampling, icing of the FSSP causes noticeable degradation of the data. Wind tunnel tests suggest that icing primarily causes a shift of the spectrum to smaller sizes, but examination of field data also shows a definite decrease of concentration with time. Apparently, the erroneous measurements are caused by wetting or icing of the prism and mirror, and also by the accumulation of ice on the front of the sampling tube. No attempt has been made to correct the data for these problems, due to the variable results found in the wind tunnel tests. Therefore, even when the concentrations have been corrected for coincidence errors, the FSSP data are definitely not trustworthy beyond a few minutes into a cloud penetration, and the reliability might be questionable even in the first few minutes.

Cloud Particle Camera (CPC)

Cloud particle concentrations, sizes and types are determined by the Cannon cloud particle camera which photographs atmospheric particles *in situ* (Cannon, 1974). The size range measured by the sailplane CPC is 16 μm to 48 mm diameter, and the sampling volume increases with the particle size. For photographic images $\geq$ 170 μm diameter, water droplets can be distinguished from ice particles by the two-dot method (i.e., separation between images of the two flashlamps formed by refraction in the water drop is a measure of the drop's size). The camera has a film capacity of 3200 frames, equivalent to 27 minutes of exposure time at the maximum rate of 2 frames per second.

About the only flight-related difficulty encountered with the CPC occurs when the airspeed is incorrectly measured. This affects the synchronization of the rotating mirror with the speed of the sailplane, which is necessary to allow stop-action photography of the particles passing through the sampling volume. An incorrect airspeed will blur the images on the film, while the complete loss of the airspeed signal, as may be caused by icing of the pitot tube, will cause blank frames on the film since the rotating mirror and the flashlamps will cease to operate. This problem has only occurred a few times during conditions of prolonged exposure to cloud at low temperatures and is easily detected in examination of the film along with the true airspeed data trace.

APPENDIX C

NCAR QUEEN AIR INSTRUMENTATION

Only those instruments related to the data presented in this Note are listed below. A more complete list of the Queen Air instrumentation, specifications and characteristics is being prepared by C. Biter for publication in an NCAR Technical Note.

Temperature. A Rosemount temperature probe (Model 102E2AL) is used on both aircraft and has an accuracy of ±0.5°C.

Dew point. A Cambridge dew point (or frostpoint) hygrometer (Model 137) is used on both aircraft and has an accuracy of ±0.5°C. Occasionally the dew point data have oscillations due to various sources.

Static pressure. A Rosemount variable capacitance probe (Model 1301) measures pressure to an accuracy of ±1.0 mb on both aircraft.

Vertical velocity. On 304D a fixed vane gust probe and an INS are used to calculate vertical velocities. Accuracy is ± 1 m s^{-1}.

On 306D measured aircraft characteristics and an INS are used to calculate vertical velocities. Comparison of this computational technique with one using a fixed vane gust probe (as on 304D) showed differences less than 1 m s^{-1}. But, although accuracy of the 306D system is comparable to the 304D system, it applies only to those situations where large variations in vertical velocities occur at frequencies less than 0.3 Hz ($\gtrsim$260 m at a true airspeed of 80 m s^{-1}).

Descriptions and detailed discussions of vertical velocities calculated from these techniques are given in Kelly and Lenschow (1978) and Lenschow et al. (1978).

Horizontal winds. With a combination of information from the gust probe sensors (fixed vane on 304D and rotating vane on 306D), the differential pressure flow angle sensor, and the INS, horizontal wind velocities can be calculated within ± 1 m s^{-1} with an additional error of 0.5 m s^{-1} hr^{-1} due to drift of the INS with time. A detailed discussion of air motion measurements is presented in Lenschow et al. (1978).

REFERENCES

Byers, H. R., and R. R. Braham, Jr., 1949: *The Thunderstorm*. Washington, D.C., U.S. Government Printing Office, 287 pp.

Cannon, T. W., 1974: A camera for photography of atmospheric particles from aircraft. *Rev. Sci. Instrum. 45*, 1448-1455.

Dye, J. E., and V. Toutenhoofd, 1973: Measurements of the vertical velocity of air inside cumulus congestus clouds. *Preprints Eighth Conf. on Severe Local Storms*, Denver, Amer. Meteor. Soc., 33-34.

Eccles, P. J., 1975: Developments in radar meteorology in the National Hail Research Experiment to 1973. *Atmos. Tech. Winter 1974-75*, NCAR, 34-45.

Foote, G. B., R. C. Srivastava, J. C. Fankhauser, F. I. Harris, T. J. Kelly, R. E. Rinehart, C. G. Wade, P. J. Eccles, E. T. Garvey, M. E. Solak, R. L. Vaughan, B. E. Weiss and R. J. Wolski, 1976: Final Report - National Hail Research Experiment Randomized Seeding Experiment, 1972-1974. Volume IV: Radar Summary. NCAR, 326 pp.

Heymsfield, A. J., P. N. Johnson, and J. E. Dye, 1978: Observations of moist adiabatic ascent in northeast Colorado cumulus congestus cloud. *J. Atmos. Sci., 35*, 1689-1703.

Kelly, T. J., and D. H. Lenschow, 1978: Thunderstorm updraft velocity measurements from aircraft. *Preprints Fourth Symposium on Meteor. Observ. and Instrum.*, Denver, Amer. Meteor. Soc., 474-478.

Knollenberg, R. G., 1976: Three new instruments for cloud physics measurements: The 2-D spectrometer, the forward scattering spectrometer probe, and the active scattering aerosol spectrometer. *Preprints Int. Conf. on Cloud Physics*, Boulder, Amer. Meteor. Soc., 554-561.

Lenschow, D. H., C. A. Cullian, R. B. Friesen and E. N. Brown, 1978: The status of air motion measurements on NCAR aircraft. *Preprints Fourth Symposium on Meteor. Observ. and Instrum.*, Denver, Amer. Meteor. Soc., 443-438.

Ryan, B. F., E. R. Wishart, and D. E. Shaw, 1976: The growth rates and densities of ice crystals between -3°C and -21°C. *J. Atmos. Sci., 33*, 842-850.

Scott, B. C., and P. V. Hobbs, 1977: A theoretical study of the evolution of mixed-phase cumulus clouds. *J. Atmos. Sci., 34*, 812-826.